cmgh
CELLULAR AND MOLECULAR GASTROENTEROLOGY AND HEPATOLOGY

ORIGINAL RESEARCH

A Proximal-to-Distal Survey of Healthy Adult Human Small Intestine and Colon Epithelium by Single-Cell Transcriptomics

Joseph Burclaff,[1,2,*] R. Jarrett Bliton,[3,*] Keith A. Breau,[4] Meryem T. Ok,[3] Ismael Gomez-Martinez,[4] Jolene S. Ranek,[5] Aadra P. Bhatt,[1,2,6] Jeremy E. Purvis,[5,7] John T. Woosley,[8] and Scott T. Magness[1,2,3,4,6]

[1]Department of Medicine, [2]Center for Gastrointestinal Biology and Disease, [3]Joint Department of Biomedical Engineering, University of North Carolina at Chapel Hill/North Carolina State University, Chapel Hill, North Carolina, [4]Department of Cell Biology and Physiology, [5]Curriculum in Bioinformatics and Computational Biology, [6]Lineberger Comprehensive Cancer Center, [7]Department of Genetics, [8]Department of Pathology and Laboratory Medicine, University of North Carolina at Chapel Hill, Chapel Hill, North Carolina

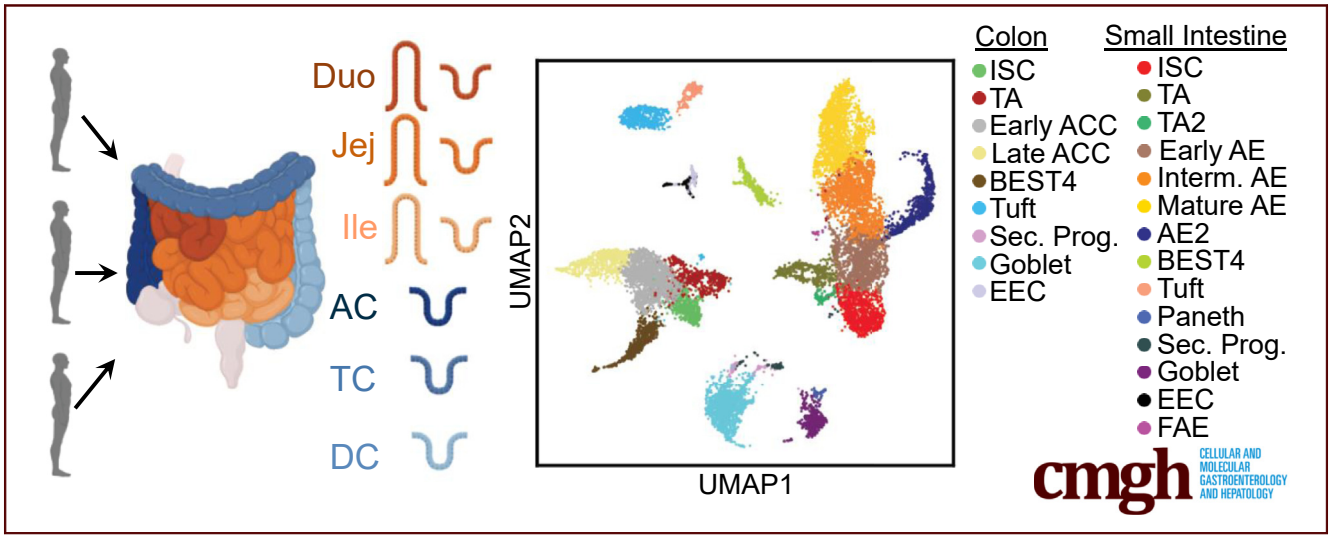

SUMMARY

We present a single-cell transcriptomic atlas of epithelial cells from the duodenum to descending colon using 3 intact healthy adult organs. Thorough analyses provide differentially expressed/functional genes, regional differences, murine model comparisons, and gene sets highlighting potential receptor-ligand and drug-target interactions

BACKGROUND & AIMS: Single-cell transcriptomics offer unprecedented resolution of tissue function at the cellular level, yet studies analyzing healthy adult human small intestine and colon are sparse. Here, we present single-cell transcriptomics covering the duodenum, jejunum, ileum, and ascending, transverse, and descending colon from 3 human beings.

METHODS: A total of 12,590 single epithelial cells from 3 independently processed organ donors were evaluated for organ-specific lineage biomarkers, differentially regulated genes, receptors, and drug targets. Analyses focused on intrinsic cell properties and their capacity for response to extrinsic signals along the gut axis across different human beings.

RESULTS: Cells were assigned to 25 epithelial lineage clusters. Multiple accepted intestinal stem cell markers do not specifically mark all human intestinal stem cells. Lysozyme expression is not unique to human Paneth cells, and Paneth cells lack expression of expected niche factors. Bestrophin 4 $(BEST4)^{+}$ cells express Neuropeptide Y (NPY) and show maturational differences between the small intestine and colon. Tuft cells possess a broad ability to interact with the innate and adaptive immune systems through previously unreported receptors. Some classes of mucins, hormones, cell junctions, and nutrient absorption genes show unappreciated regional expression differences across lineages. The differential expression of receptors and drug targets across lineages show biological variation and the potential for variegated responses.

CONCLUSIONS: Our study identifies novel lineage marker genes, covers regional differences, shows important differences between mouse and human gut epithelium, and reveals insight into how the epithelium responds to the environment and drugs. This comprehensive cell atlas of the healthy adult human intestinal epithelium resolves likely functional differences

across anatomic regions along the gastrointestinal tract and advances our understanding of human intestinal physiology. *(Cell Mol Gastroenterol Hepatol 2022;13:1554–1589; https://doi.org/10.1016/j.jcmgh.2022.02.007)*

Keywords: scRNAseq; Cell Atlas; Intestinal Stem Cell; Paneth Cell; BEST4.

Colloquially called the *gut*, the small intestine (SI) and colon are distinct organs with overlapping and unique roles in maintaining health. The gut lumen is lined by epithelial stem and differentiated cells that renew weekly.[1] Cellular roles include absorption, ion balance, hormone production, mucus production, and signaling through the luminal–epithelial–immune axis. Although physiological functions vary along the gut, how lineages differ across the SI–colon axis is poorly understood.

Single-cell RNA sequencing (scRNAseq) approaches have provided unprecedented transcriptomic resolution of cells and have shown unappreciated cellular heterogeneity. Human intestinal scRNAseq studies often analyze individual regions, with studies on adult colonic,[2–5] ileal,[6–8] and duodenal[9] epithelium available. One study compared adult human ileum and regionally unspecified colon,[6] and a recent report compiled a regional mosaic using multiple donor samples yet had few donors for some regions and provided a limited epithelial analysis.[10] Several human gut regions have sparse scRNAseq analysis available, with no scRNAseq studies analyzing differences among regions within the human SI or colon.

Here, we comprehensively survey adult human gut epithelium using transplant-grade organs. scRNAseq libraries were prepared from epithelial cells from duodenum, jejunum, ileum, and ascending (AC), transverse (TC), and descending (DC) colon from 3 donors. This experimental design provides a robust library that avoids intradonor batch effects and allows comparisons between all 6 regions across the same 3 individual patients. Using this data set, we probe understudied human lineages including Paneth cells (PCs), Bestrophin 4 (BEST4)$^+$ cells, and follicle-associated epithelium (FAE). We define comprehensive transcriptional signatures for lineages along the entire gut and generate regional atlases of functional gene families. We further probe how lineages might be affected by extrinsic signaling through mapping receptor families and analyzing primary gene targets of approved drugs.

Results

Sample Processing

We define SI and colon as organs, and duodenum, jejunum, ileum, AC, TC, and DC as regions. Intestinal tracts were obtained from 3 disease-free organ donors (Figures 1*A* and 2), with a pathologist verifying healthy mucosa. Epithelium from each region was dissociated to single cells using cold protease to preserve RNA integrity and cells were flow-sorted to exclude dead cells and doublets before sequencing. Cells from each region were stained with cell hashtag antibody-oligo conjugates[11,12] to multiplex regions for library preparation and sequencing, then cells from all regions per donor were sorted concurrently to avoid intradonor batch effects and reduce cost. Readouts were filtered for minimum and maximum total counts and maximum mitochondrial gene reads to exclude transcriptomes of low-read count cells, multiplets, and likely dead cells, respectively. Hashtag deconvolution allowed for more stringent filtering against clusters and contaminating messenger RNA (mRNA) than available in other studies, with cells positive for multiple hashtags removed to filter out likely multiplets or cells contaminated with RNA from other cells. After filtering, transcriptional readouts for 12,590 total cells were obtained (Figure 2), with consistent read depth (11,378 reads per cell) and gene counts (2851 genes per cell) seen across regions.

Donor data sets were individually processed and then combined. Principal components were integrated with Harmony[13] before dimensional reduction and Leiden clustering.[14] Most lineages formed SI- and colon-specific clusters, suggesting functional differences between organs. One cluster expressed PC and goblet cell (GC) markers, so subclustering resolved these lineages (Figure 3). Our final data set identifies all lineages by organ (Figure 1*B*). The integrated data set shows overlapping cell distributions from each donor and region within all major lineages, showing that postsequencing hashtag deconvolution preserves transcriptomic features across batches (Figure 1*C*–*E*). Cell counts for each region show that all 3 donors contributed approximately one third (33%) of the total cells analyzed for each region and no individual donor provided the majority of cells for any specific region, with each donor providing 20%–48% of the total cells for every region (Figure 2).

To define transcriptional signatures for each lineage, we calculated differentially expressed genes (DEGs) in both organs for each lineage (Supplementary Table 1). We also identified DEGs consistently enriched across all 6 regions and in all 3 donors, defining DEGs that are lineage-specific regardless of position in the SI or colon (Supplementary Table 2). This statistical evaluation provides previously unavailable transcriptional signatures for all lineages across the human SI and colon epithelium (Figure 1*F* and *G*).

***Authors share co-first authorship.**

Abbreviations used in this paper: **AC, ascending colon; ACC, absorptive colonocyte; AE, absorptive enterocyte; BEST4$^+$, Bestrophin 4; DC, descending colon; DEG, differentially expressed genes; dPBS, Dulbecco's phosphate-buffered saline; EEC, enteroendocrine cell; FAE, follicle-associated epithelium; GC, goblet cell; GI, gastrointestinal; IBD, inflammatory bowel disease; icGC, intercrypt goblet cell; IL, interleukin; ISC, intestinal stem cell; LPS, lipopolysaccharide; M-cell, microfold cell; mRNA, messenger RNA; PAGA, partition-based graph abstraction; PC, Paneth cell; scRNAseq, single-cell RNA sequencing; SI, small intestine; TA, transit amplifying; TC, transverse colon.**

Most current article

2352-345X
https://doi.org/10.1016/j.jcmgh.2022.02.007

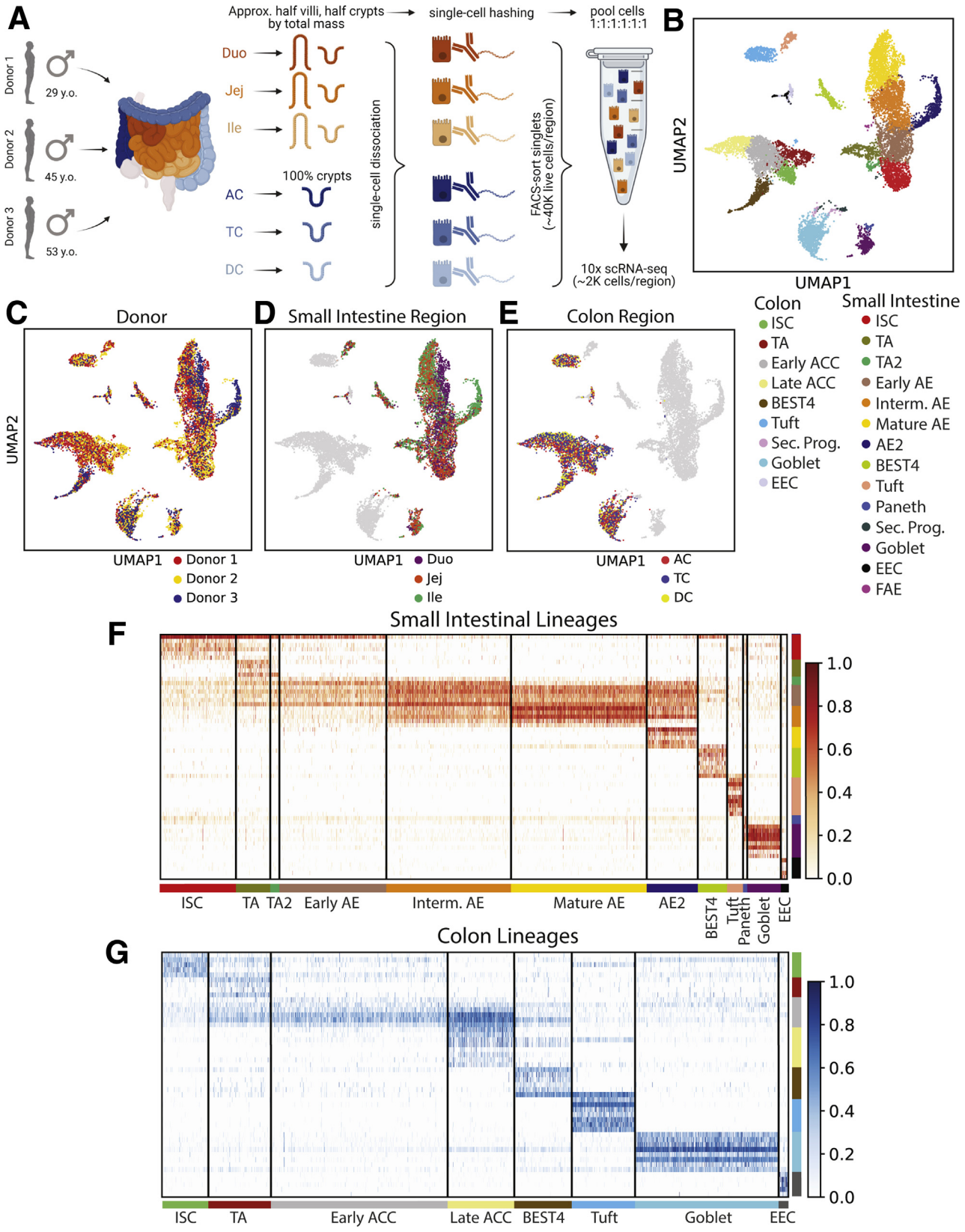

Figure 1. Sample processing. (*A*) Schematic for isolating single epithelial cells from 6 intestinal regions for 3 donors and then using hashtag antibodies to sequence cells from all regions side-by-side. (*B*) UMAP of all analyzed cells in 25 lineage clusters. See Figure 19 for clearly marked clusters. (*C–E*) UMAP of all cells colored by (*C*) donor or (*D* and *E*) region. (*F* and *G*) Heatmaps showing unique markers for major lineages in (*F*) SI and (*G*) colon. See Supplementary Table 1 for total DEGs for each lineage. Schematics in panel *A* were created with BioRender.com. Duo, Duodenum; FACS, fluorescence-activated cell sorter; Ile, Ileum; Interm, intermediate; Jej,Jejunum; Sec. Prog., Secretory Progenitor; UMAP, Uniform Manifold Approximation and Projection.

A

Donor Characteristics					
Donor	Sex	Age	Race	BMI	Intestinal Status
Donor 1	Male	29	White	36.4	Healthy
Donor 2	Male	45	White	52.2	Healthy
Donor 3	Male	53	African American	25	Healthy

B

Cells collected per donor region				
	Total Cells	Donor 1	Donor 2	Donor 3
Duodenum	2115	687	423	1005
Jejunum	2612	869	961	782
Ileum	2609	918	1097	594
Asc. Colon	1746	733	557	456
Trans. Colon	2171	567	1042	562
Desc. Colon	1337	556	385	396

C

Small intestinal lineages collected per donor				
	Total Cells	Donor 1	Donor 2	Donor 3
Mature AE	1569	607	372	590
Intermediate AE	1443	631	302	510
EArly AE	1237	455	498	284
ISC	873	239	448	186
AE2	591	35	113	443
TA	397	111	259	27
Goblet	388	77	184	127
BEST4	339	148	73	118
Tuft	184	81	94	9
TA2	105	29	67	9
EEC	72	19	25	28
Sec. Progenitors	70	34	12	24
Paneth	49	8	15	26
FAE	19	0	19	0

D

Colonic lineages collected per donor				
	Total Cells	Donor 1	Donor 2	Donor 3
Early ACC	1464	783	533	148
Goblet	1189	157	435	597
Late ACC	552	292	126	134
Tuft	524	191	230	103
TA	518	140	344	34
BEST4	477	92	81	304
ISC	385	178	171	36
EEC	82	15	22	45
Sec. Progenitors	63	8	42	13

E

		Small Intestinal lineages per donor region								
		Donor 1			Donor 2			Donor 3		
Cell Type	Total #	Duodenum	Jejunum	Ileum	Duodenum	Jejunum	Ileum	Duodenum	Jejunum	Ileum
Mature Abs. Enterocytes	1569	43	192	372	20	33	319	278	311	1
Intermediate Abs. Enterocytes	1443	262	164	205	15	42	245	368	138	4
Early Abs. Enterocytes	1237	190	171	94	116	246	136	141	99	44
Stem Cells	873	90	96	53	112	299	37	90	75	21
Abs. Enterocytes 2	591	0	13	22	30	71	12	2	0	441
Transit Amplifying Cells	397	40	50	21	29	69	161	17	4	6
Goblet Cells	388	10	44	23	44	106	34	28	65	34
BEST4 Cells	339	18	68	62	12	28	33	49	45	24
Tuft Cells	184	8	29	44	21	25	48	2	5	2
Transit Amplifying 2	105	10	17	2	11	15	41	3	5	1
Enteroendocrine Cells	72	11	5	3	8	10	7	10	14	4
Secretory Progenitors	70	4	14	16	0	7	5	10	9	5
Paneth Cells	49	1	6	1	1	8	6	7	12	7
FAE Cells	19	0	0	0	4	2	13	0	0	0

F

		Colon lineages per donor region								
		Donor 1			Donor 2			Donor 3		
Cell Type	Total #	Asc. Colon	Trans. Colon	Desc. Colon	Asc. Colon	Trans. Colon	Desc. Colon	Asc. Colon	Trans. Colon	Desc. Colon
Late Abs. Colonocytes	552	93	99	100	22	82	22	29	76	29
Early Abs. Colonocytes	1464	314	254	215	128	283	122	33	64	51
Stem Cells	385	68	72	38	63	79	29	10	12	14
Transit Amplifying Cells	518	76	29	35	55	233	56	15	12	7
Goblet Cells	1189	65	27	65	182	207	46	215	224	158
Secretory Progenitors	63	4	1	3	15	23	4	6	6	1
BEST4 Cells	477	26	28	38	21	38	22	100	111	93
Tuft Cells	524	76	55	60	65	90	75	31	39	33
Enteroendocrine Cells	82	11	2	2	6	7	9	17	18	10

Figure 2. Patient characteristics and cell counts. (*A*) Donor information. (*B*) Cells collected per donor region. (*C*) Small intestinal lineages collected per donor. (*D*) Colonic lineages collected per donor. (*E*) Small intestinal lineages per donor region. (*F*) Colonic lineages per donor region. Abs., Absorptive; Asc., Ascending; BMI, body mass index; Desc., Descending; Trans., Transverse.

Proliferative Cells

We found that human intestinal stem cells (ISCs) significantly expressed classic markers *LGR5*, *ASCL2*, *SLC12A2*, and *RGMB* (Figure 4*A* and *B*).[15–17] *SMOC2*[18] was not a DEG in SI ISCs because PCs unexpectedly were found to express it at higher levels (see Paneth Cell section). Although in situ hybridization was used in a previous report that concluded that *OLFM4* marks human colonic ISCs,[19] our results showed colonic *OLFM4* levels were higher in transit-amplifying (TA) cells (Figure 4*C*), consistent with mouse studies.[16] *RARRES2*, a retinoid-response gene with no reported association to the gut epithelium, was enriched in colon ISCs, with low SI ISC expression (Figure 4*B*).

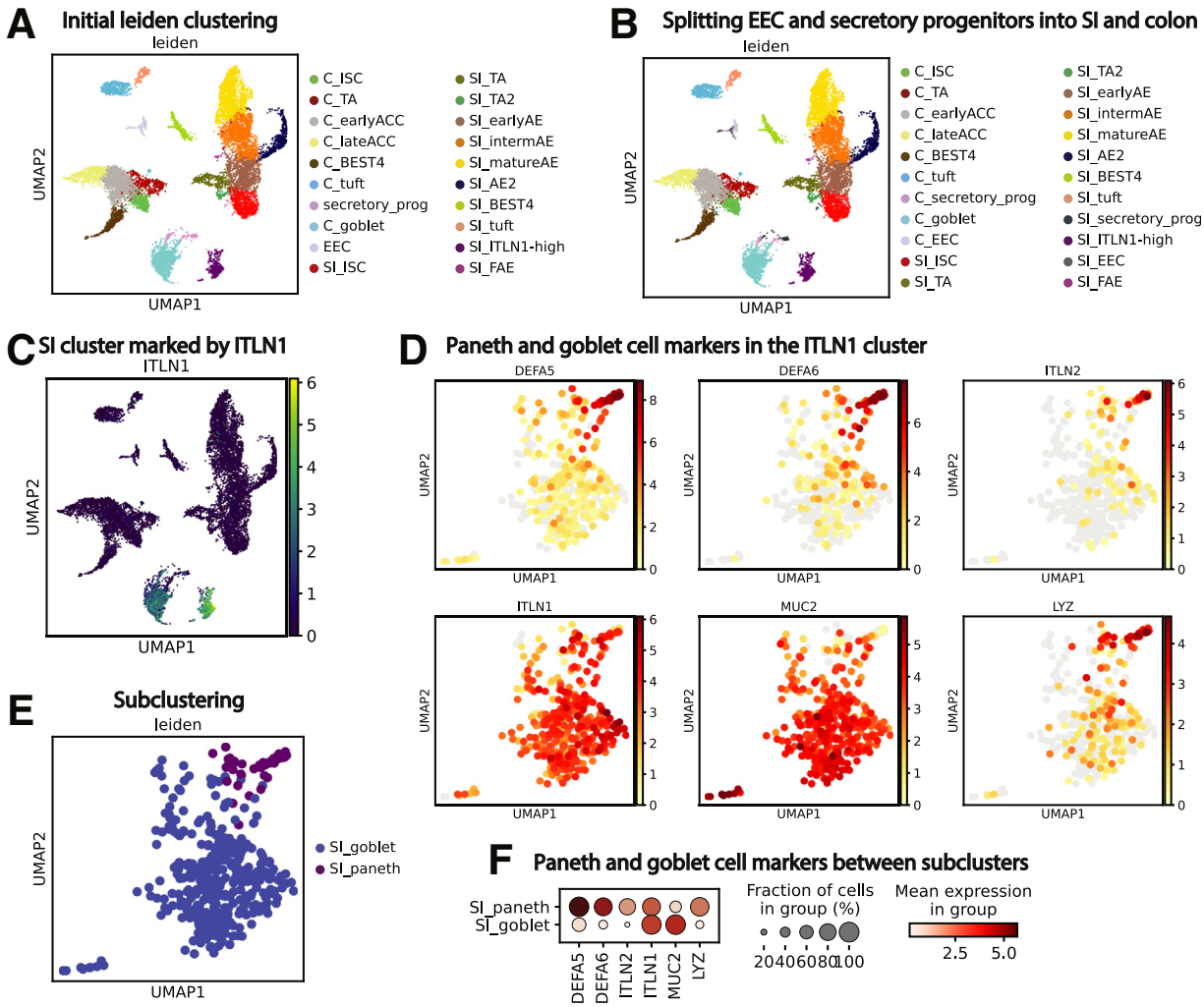

Figure 3. Determining final lineage clusters. (*A*) Initial Leiden clustering for all cells. (*B*) Splitting EEC and secretory progenitors by organ. (*C* and *D*) An *ITLN1*-high cluster, all from SI, contains cells expressing PC markers (*DEFA5*, *DEFA6*, *ITLN2*, *LYZ*) along with cells expressing the GC marker *MUC2*. (*C*) cluster defined by *ITLN1*; (*D*) UMAP expression of PC and GC markers within the *ITLN1*-high cluster. (*E*) Subclustering to define Paneth and Goblet cells. (*F*) Dotplot showing expression of classic PC and GC genes across the new PC and GC clusters. UMAP, Uniform Manifold Approximation and Projection.

SI ISCs had 68 DEGs compared with other SI clusters, whereas colon ISCs displayed 109 DEGs compared with other colon clusters (Supplementary Table 1, Figure 5). We identified 46 ISC DEGs enriched across both organs, defining an ISC transcriptional signature spanning SI and colon (Supplementary Table 2). This signature includes classic ISC markers and 30 ribosomal genes, consistent with transcriptional regulation by ribosomes shown in other stem cell populations.[20–22] To identify ISC DEGs conserved between human beings and mice, we compared our 68-gene SI ISC signature with a mouse ISC signature defined by bulk RNA sequencing of flow-sorted Leucine Rich Repeat Containing G Protein-Coupled Receptor 5 ($Lgr5^{+}$) cells.[18] Surprisingly, only 11 genes overlapped between the signatures (Figure 4*D*), although it is unclear whether this reflects species differences or the higher stringency of scRNAseq and computational analysis compared with bulk sequencing of cells sorted using a fluorescent reporter. Conserved genes included classic markers: *LGR5*, *OLFM4*, *ASCL2*, *RGMB*, *SLC12A2*, and *MYC*; genes with known ISC function: *RNF43*, *ZBTB38*, *VDR*, and *CDK6*; and 1 gene absent in ISC literature: *TRIM24*. These SI, colon, and full-gut ISC signatures underline key similarities and differences in proximal–distal human ISCs.

Leiden clustering separated SI TA cells undergoing S/G2 cell-cycle phases (TA) and M-phase (TA2) (Supplementary Tables 3 and 4). We found that DEGs shared across SI TA, SI TA2, and colon TA cells (Figure 4*E*) were involved in the cell cycle, mitochondrial biogenesis, and ribosomal RNA processing, consistent with the increased mitochondrial load and translation seen because stem cells differentiate in various systems.[20,23–25] Several organ-specific markers of differentiated lineages (Figure 6) were enriched unexpectedly in their respective SI or colon ISC and TA populations (Figure 4*F*), hinting that ISCs are transcriptionally primed for organ-specificity instead of existing in a pan-intestinal

state. This is consistent with adult rodent SI ISCs producing daughter cells specific to their originating organ when engrafted into alternative sites.[26,27] Studies defining region/organ-specific chromatin or transcriptomic differences in human ISCs were not found; thus, these genes may aid in studying early differentiation and chromatin dynamics.

Trajectory analyses computationally investigate lineage transitions and have been used previously to describe mouse physiology.[28–31] We used partition-based graph abstraction (PAGA), which analyzes transcriptomic similarity between individual cells in different clusters, to define total connection strength (connectivity) between progenitor and differentiated populations and to infer temporal lineage trajectories.[32] As expected, absorptive enterocytes (AEs) and absorptive colonocyte (ACCs) are strongly and almost exclusively connected to ISCs and TA cells,[8,33] while PCs, GCs, and enteroendocrine cells (EECs) connect strongly to the secretory progenitor population (Figure 4*G* and *H*). Consistent with murine findings, tuft cells connect weakly but exclusively to secretory progenitors in colon but not in SI.[34,35] Conversely, SI BEST4$^+$ cells connect weakly but exclusively to secretory progenitors while colonic BEST4$^+$ cells connect strongly to TA cells. Because the strength of a connection depends directly on the number of cells analyzed, future studies that enrich for secretory progenitors and immature but lineage-committed, crypt-base populations are needed to further strengthen these findings.

Predicted regional cell-cycle phase distributions[36] were analyzed in proliferative lineages (Figure 4*I–K*). ISCs showed high G1- and S-phase across regions,[6] while highly proliferative TA cells largely existed in the S and G2/M. TC showed lower proportions of TA cells in G2/M than jejunum, reflecting regional differences seen in rodents.[34] Secretory progenitors showed increasing S phase proximally to distally and higher G1 proportion than TA cells.

Paneth Cells

Murine PCs play important niche-supporting and antimicrobial roles,[37] yet little scRNAseq analysis covers human PCs. Our data include 49 human PCs, 10 times more than analyzed in recent literature.[9] PCs were defined using *DEFA5*, *DEFA6*, *ITLN2*, and *PLA2G2A* (Figure 7*A*). Because PCs cluster alongside GCs and share *LYZ* expression with BEST4$^+$ cells, classic markers were plotted to confirm PC identity (Figure 7*C*). Surprisingly, the murine marker *LYZ* was not unique to human PCs, with expression also seen in BEST4$^+$ cells and high expression in FAE (Figure 7*B*). This is consistent with *LYZ* expression found in fetal human organoids not expected to form PCs.[38] Other human intestinal scRNAseq reports also have indicated that *LYZ* mRNA is not unique to PCs, with 1 report showing that *LYZ* is not a top PC DEG[8] and another showing *LYZ* as a DEG for M cells,[10] consistent with our findings (Figure 7*B*, Supplementary Table 1). This indicates that although human PCs indeed express *LYZ*, the presence of this gene product alone is insufficient to determine PC identity or presence. Importantly, our data indicate the cells designated as PCs in a recent scRNAseq publication[6] are actually BEST4$^+$ cells because they are marked by high *LYZ*, *SPIB*, *BEST4*, and *CA7*. Similarly, the colonic Paneth-like cells reported in the study likely also are BEST4$^+$ cells. The rarity of PCs in scRNAseq data (<1% here and elsewhere[9]), and the presence of *LYZ* mRNA in other lineages in addition to PCs, highlights the precise lineage attribution needed when defining human PCs.

Murine PCs express ISC niche factors including *Wnt3*, *Wnt11*, *Tgfa*, *Egf*, *Dll1*, *Rspo1*, and *Dll4*,[29,37,39,40] but 1 report showed human PCs express no *WNT3/11*.[9] Our data confirm this and showed no measurable *EGF* or *RSPO1* and minimal *TGFA* (Figure 7*D*). *DLL1* and *DLL4* are both expressed higher in secretory progenitors (Figure 7*D*). We found no intestinal growth factors enriched in PCs (Figure 7*E*), suggesting human PCs are not major niche-supporting cells. This agrees with nonepithelial sources of WNTs and growth factors in the human niche[38,41] and echoes mouse biology, where PCs support ISCs[37] yet are unnecessary for niche maintenance.[37,42–44]

Unexpectedly, *SMOC2*, a murine ISC marker,[18] was expressed highest in PCs, with other markers shown as restricted to ISCs in mouse (*LGR5*, *ASCL2*, *RGMB*) expressed higher in human PCs than expected from the mouse data[45] (Figure 7*F*). Expression of *SMOC2* mRNA in human PCs was visualized using in situ hybridization, with obvious overlap seen between *SMOC2* and LYZ protein (Figure 7*F*). ISC-PC doublets could provide a possible explanation for these ISC genes presenting in PCs, yet the lack of many other ISC markers in PCs, notably the nearly complete absence of *OLFM4*, opposes this hypothesis. *LGR5*, *SMOC2*, and *ASCL2* function in WNT reception,[15,46–48] suggesting human PCs receive WNT signals instead of providing WNT signals.[37] PC unique *FZD9* expression further supports a WNT-receptive PC role (Figure 7*H*).

Despite striking differences between mouse and human PCs, both supply antimicrobial gene products. Six of the 10 highest expressed SI antimicrobial peptides are PC-enriched (Figure 7*I*). Because antimicrobial genes comprise half of human PC DEGs (Supplementary Table 1), PCs largely appear to function to protect the ISC niche.[49]

BEST4$^+$ Cells

Recent human scRNAseq studies have described a novel intestinal lineage, absent in mice, expressing *BEST4*, *SPIB*, and *CA7*,[5] with SI-specific *CFTR*[9,10] and colon-specific *OTOP2*. Because these cells often are described by their expression of *BEST4*, here we label these SI and colon clusters BEST4$^+$ cells. Our DEGs encompassed all of the previously defined markers for BEST4$^+$ cells (Figure 8*A*). By comparing with diffusion pseudotime, which infers trajectory,[50] our data suggested that *BEST4* is only expressed to high levels as the cells mature (Figure 8*B*), and this was confirmed with in situ hybridization, with *BEST4*-high cells never seen in the proliferative crypts of SI (Figure 8*C*) or colon (Figure 8*D*). In line with previous literature,[9,10] cystic

fibrosis transmembrane conductance regulator (CFTR) protein was shown to mark the apical tips of SI BEST4^{+} cells (Figure 8*C*) but not colonic BEST^{+} cells (Figure 8*D*). With the function of BEST4^{+} cells largely unknown, DEGs were used to predict their physiological roles. DEGs included *GUCA2A* and *GUCA2B*[5], which act as prohormones regulating

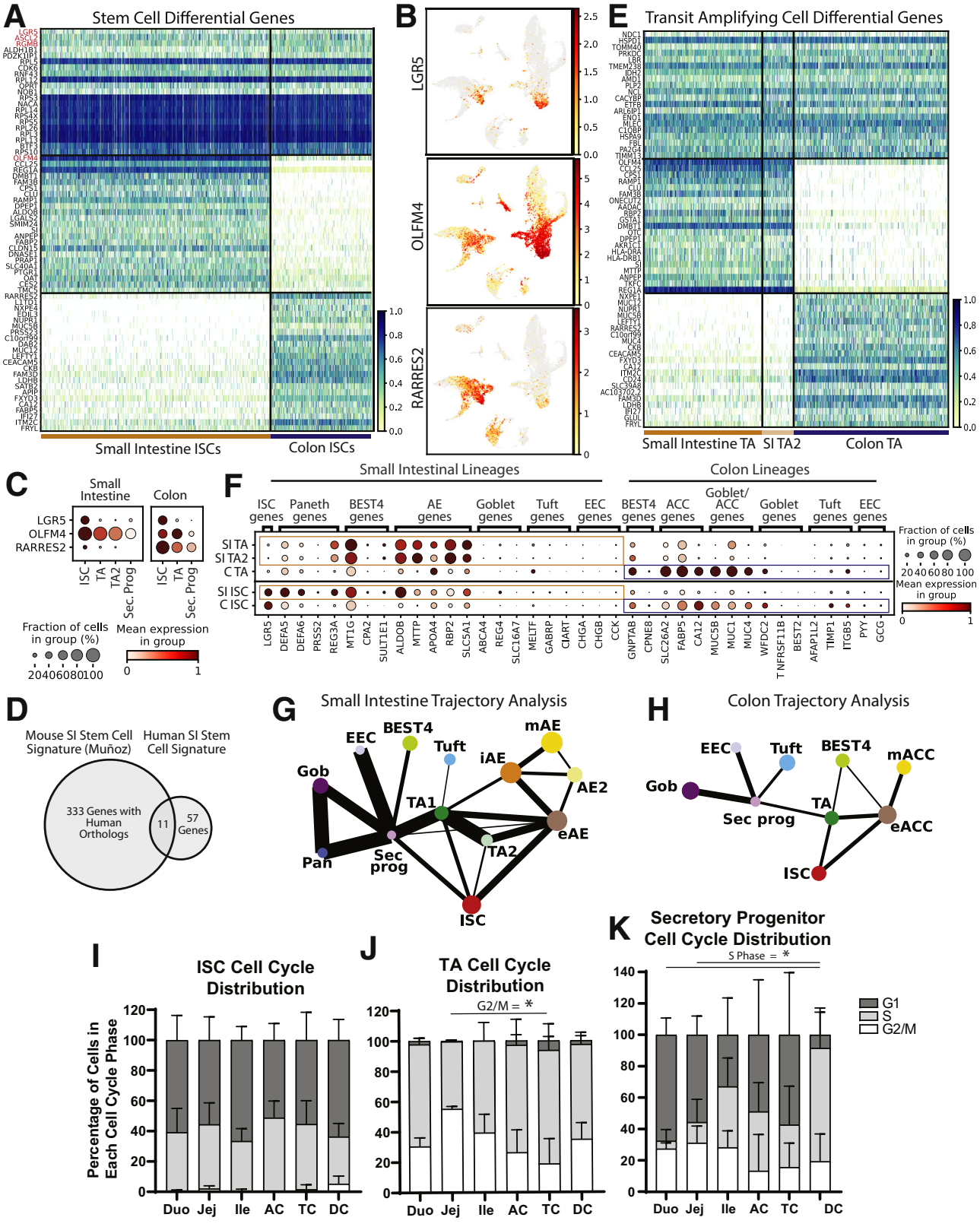

satiety.[51] Consistent with a previous report, we found these genes expressed in SI and colon BEST4$^+$ cells,[9] yet our database furthers this finding by showing that both genes are expressed higher in SI BEST4$^+$ cells than in colonic BEST4$^+$ cells (Figure 8*E*).

We identified 2 previously unreported secreted peptides, *NPY* and *BMP3*, specifically in SI BEST4$^+$ cells (Figure 8*E*). *NPY* expression is unexpected in intestinal epithelium,[52] and gut *BMP3* is largely studied for its antitumor roles.[53] Similar to *BEST4*, we found that *NPY*, *GUCA2A*, and *GUCA2B* expression increased with BEST4$^+$ cell maturation, while *BMP3* was expressed independently of maturation (Figure 8*F*). Interestingly, EECs express receptors for all 4 genes, suggesting EEC–BEST4$^+$ cell crosstalk (Figure 8*E*).

Because *NPY* is proposed to affect gastrointestinal (GI) motility and energy homeostasis,[54,55] we probed if *NPY* correlated with genes induced after meals. We found strong positive correlations across SI regions for each donor between SI BEST4$^+$ cell *NPY* expression and AE expression of *SI* (R = 0.82) and *APOA4* (R = 0.86), which are induced by dietary sugar[56] and fat[57] (Figure 8*G*). We found further positive correlations with AE genes involved in dietary metabolism (Supplementary Table 5), and negligible correlation with housekeeping genes *ACTB* (R = -0.22) or *GAPDH* (R = -0.08), suggesting postprandial induction of SI BEST4$^+$ *NPY* expression. Further SI BEST4$^+$ cell DEGs included *ADRA2A* and *CHRM3*, receptors involved in intestinal motility[58] (Supplementary Table 1), reinforcing that SI BEST4$^+$ cells regulate intestinal motility after meals.

BEST4$^+$ cells likely absorb dietary heavy metals. Metallothioneins, which bind heavy metals and prevent toxicity,[59–61] were described in colonic BEST4$^+$ cells,[5] yet we found 7 metallothioneins specifically enriched in SI BEST4$^+$ cells (Figure 8*H*) alongside *STEAP2*, a metalloreductase for copper and iron,[62] suggesting SI BEST4$^+$ cells maintain SI metal ion homeostasis.[61–63] Our data indicate BEST4$^+$ cells perform diverse roles within the intestinal epithelium, laying the groundwork for functional studies.

Tuft Cells

Tuft cells are chemosensory cells that regulate type 2 immune reactions[64–66] in the intestinal epithelium through interleukin (IL)25 signaling in response to pathogenic metabolites.[67–69] SI and colon tuft cells share many classic markers[9,70] (Figure 9*A*, Supplementary Tables 1 and 2). *DCLK1*, a key murine marker,[69] was not observed as a DEG. *SUCNR1*, a G-protein–coupled receptor mediating SI IL25 release,[71] was negligible in the colon, suggesting SI and colon tuft cells differentially detect succinate-producing pathogens (Figure 9*B* and *C*). Colonic tuft cells likely detect umami-chemosensory cues (eg, microbe-derived free amino acids) with heterodimeric umami taste receptor subunits *TAS1R1* and *TAS1R3* (Figure 9*B* and *C*).[72] Downstream taste signal transduction genes are enriched in SI and colon tuft cells,[64,65] with SI-specific *GNAT3* likely activating *PDE4D* to decrease intracellular cyclic adenosine monophosphate/cyclic guanosine monophosphate (cAMP/cGMP)[73] (Figure 9*B*). This suggests human SI tuft cells have multiple responses to succinate-producing microbes (eg, *Nippostrongylus brasiliensis*), whereas colonic tuft cells respond to other microbial taxa.

Beyond triggering type 2 immunity, tuft cell DEGs allow broad interaction with the adaptive and innate immune systems. Tuft cell DEGs implicate ubiquitin-mediated proteasome degradation, with enriched Skp, Cullin, F-box containing complex (SCF) complex components (*SKP1*, *CUL3*, *FBXO32*, *RBX1*) initiating exogenous antigen processing for presentation[74,75] to the major histocompatibility complex 1 antigen presentation complex (Figure 9*D*). This suggests tuft cells interact with the adaptive immune system after luminal stimuli. Human tuft cells also uniquely express unappreciated Toll-like receptors (*TLR9*, *TLR5*, and *TLR4*), which bind bacterial/viral DNA, flagellin, and lipopolysaccharide (LPS), respectively (Figure 9*D*).[76–79] Expression of the LPS co-receptor *CD14* across tuft cells[77] (Figure 9*D*) supports this novel role in bacterial-related immune responses.

Tuft cells show possible autoregulatory mechanisms for these pathogen-response pathways. Tuft cells express heterodimeric IL25-specific receptor components (Figure 9*D*), which may create a positive feedback loop to amplify IL25 signaling.[80] *SIGIRR* may also negatively autoregulate the Toll-like receptor 4–LPS response.[81–83] These implicate tuft cells as dynamic sentinels linking luminal contents to the immune system.

Tuft cells produce antimicrobial peptides in the SI to complement those produced by PCs (Figure 7*G*). In the colon, which lacks PCs, tuft cells express 6 of the top 10 colonic antimicrobial peptides (Figure 9*E*). Human and murine tuft cells also produce neuromodulatory and immunomodulatory compounds. We found genes necessary for acetylcholine synthesis, communication with neurons,[84] and enzymes involved in eicosanoid and prostaglandin D_2 production, which broadly regulate inflammation[85]

Figure 4. (***See previous page***). **Proliferative crypt populations.** (*A*) Heatmap of DEGs in ISCs vs other lineages (*top*; red: classic markers), SI vs colon ISCs (*middle*), and colon vs SI ISCs (*bottom*). (*B*) UMAP of *LGR5*, *OLFM4*, and *RARRES2* expression. (*C*) Dotplot showing expression of *LGR5*, *OLFM4*, and *RARRES2* across proliferative lineages of the SI (*left*) and colon (*right*). (*D*) Venn diagram showing overlap between our human ISC signature and a previously described murine signature. (*E*) Heatmap of DEGs in TA cells vs other lineages (*top*), SI vs colon TA cells (*middle*), and colon vs SI TA cells (*bottom*). (*F*) Dotplot showing DEGs defined in SI- or colon-specific mature lineages expressing within organ-delineated ISCs and TA cells. (*G* and *H*) PAGA showing connectivity between major lineages in (*G*) SI and (*H*) colon to infer the maturation trajectory. *Line thickness* represents connectivity strength. (*I–K*) Regional cell-cycle phase distribution in (*I*) ISCs, (*J*) TA cells, and (*K*) secretory progenitors. C, Colon; Duo, Duodenum; eACC, Early Absorptive Colonocytes; eAE, Early Absorptive Enterocytes; Gob, Goblet; iAE, Intermediate Absorptive Enterocytes; Ile, Ileum; Jej, Jejunum; mACC, Mature Absorptive Colonocytes; mAE, Mature Absorptive Enterocytes; Pan, Paneth; Sec. prog., Secretory Progenitor.

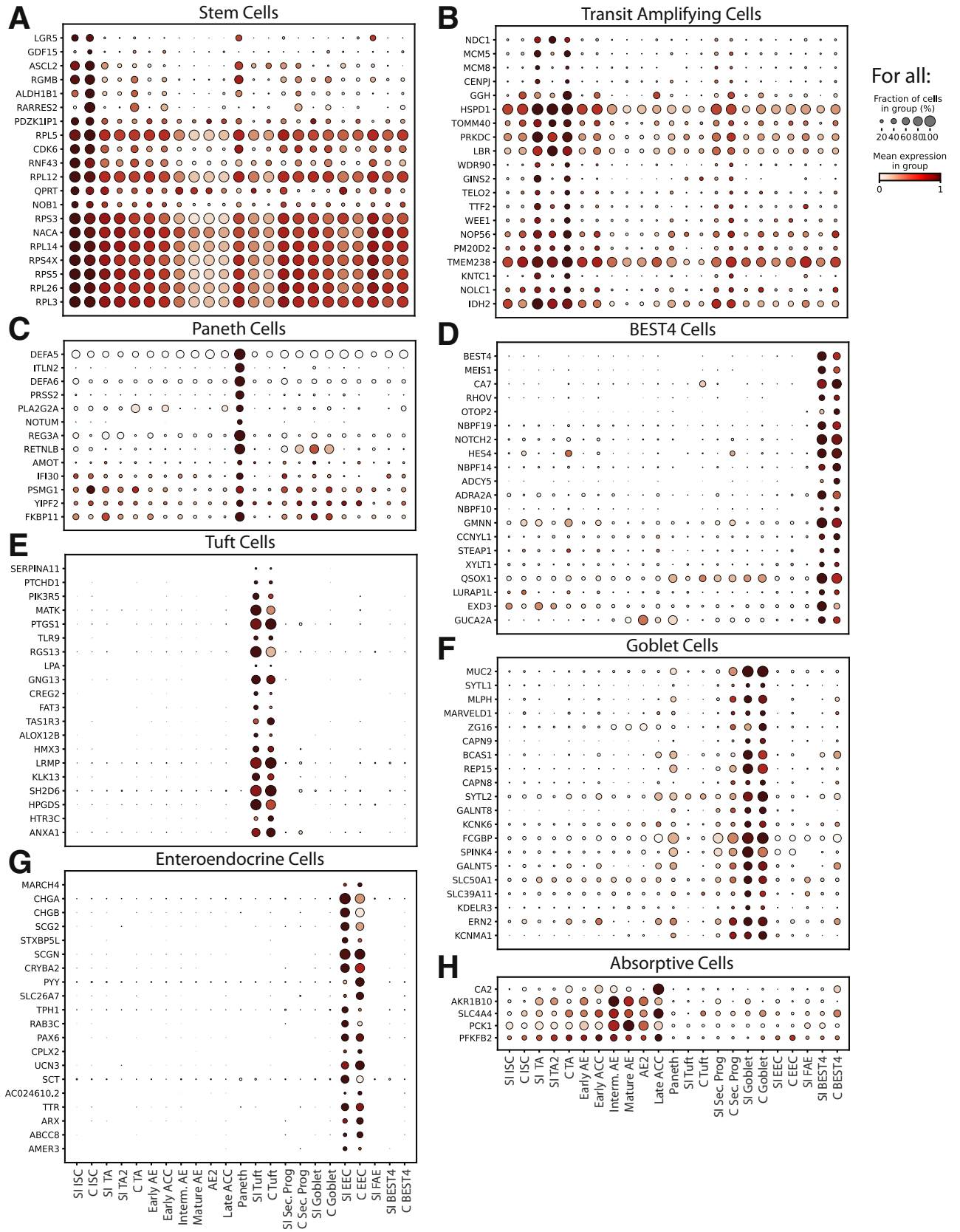

Figure 5. DEG dotplots for each lineage. Dotplots showing expression of top 20 DEGs for each lineage, as sorted by expression fold-change above the cluster with the next highest expression. DEGs included are genes significantly enriched in the lineage in both the SI and colon (if applicable).

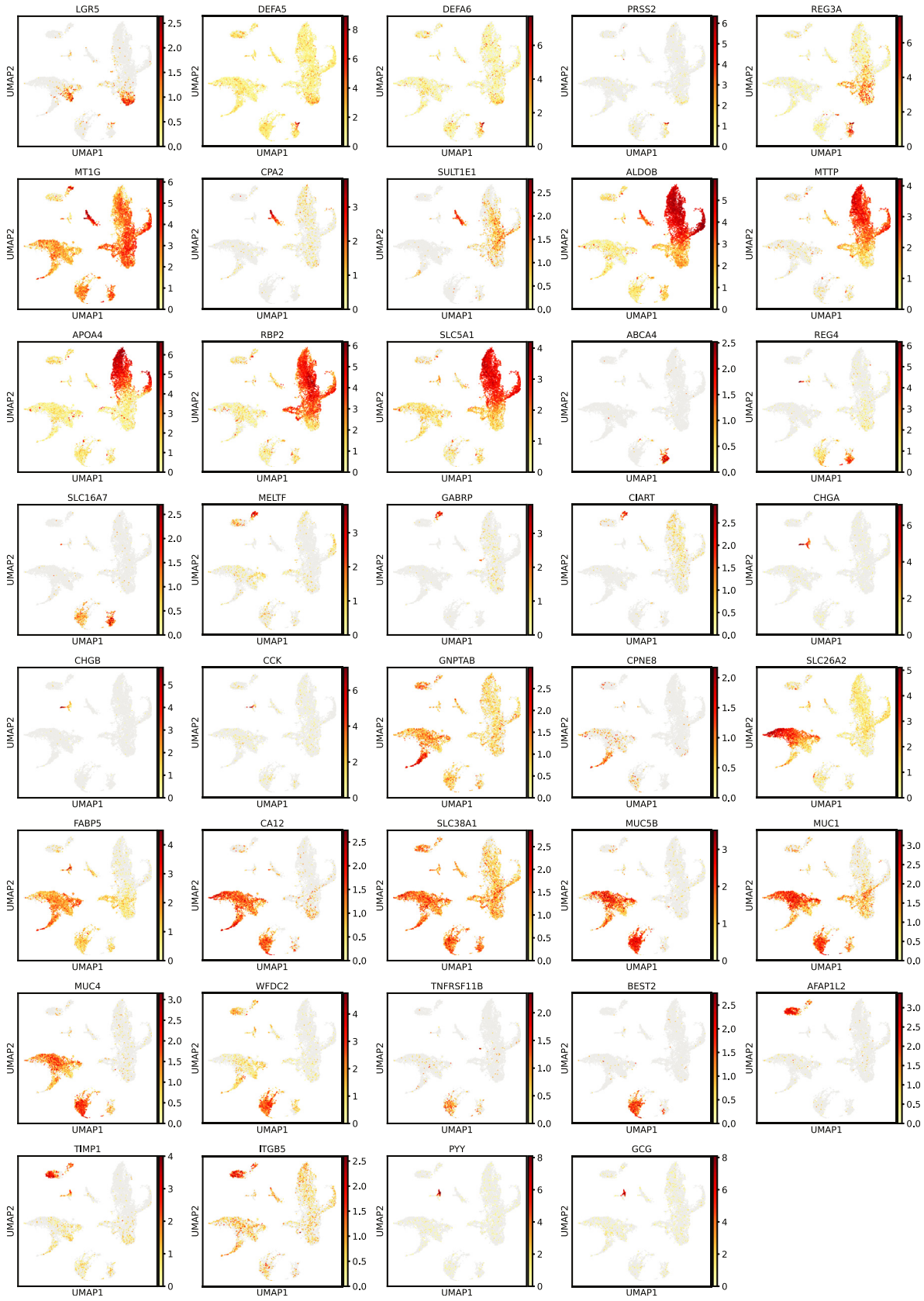

Figure 6. Organ-specific lineage DEGs. Relating to Figure 4*F*, UMAPs showing expression of DEGs from mature lineages found to be more highly enriched in SI or colon ISCs and TA cells. UMAP, Uniform Manifold Approximation and Projection.

(Figure 9*F*). These analyses suggest tuft cells regulate luminal microbes, communicate with the nervous system, and affect systemic immune responses.

Goblet Cells

GCs produce membrane-bound and secreted mucin glycoproteins that lubricate the gut, act in signaling, support

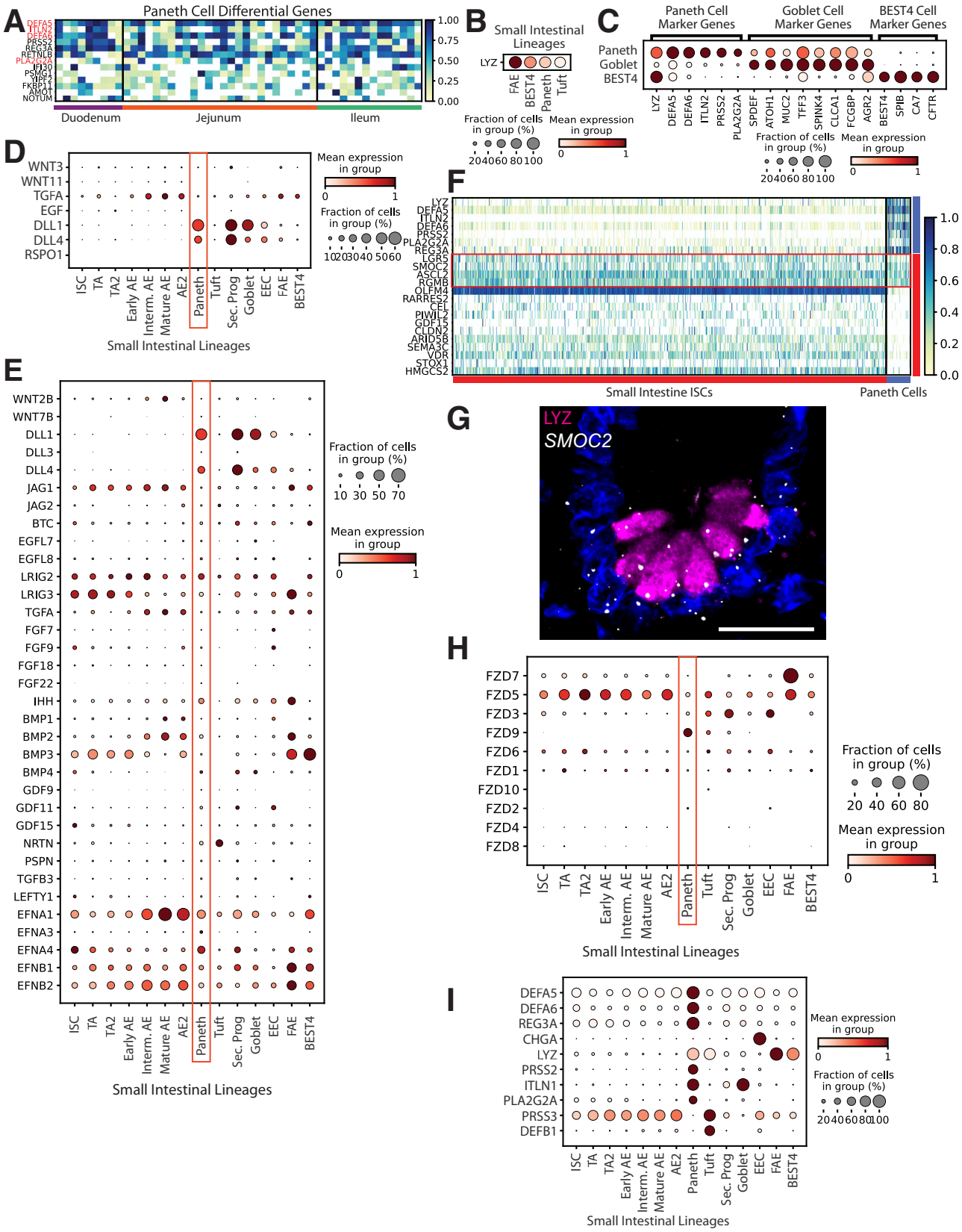

commensal bacteria, and form the protective mucus barrier.[67,86–88] DEGs include classic markers *CLCA1*, *MUC2*, and *TFF3*, with colonic GCs expressing higher *WFDC2*, consistent with previous findings[5] (Figure 10*A*). Pathway enrichment analysis of DEGs confirmed GCs principally act in mucus production and secretion, with top-enriched pathways including glycosylation, Golgi/Endoplasmic Reticulum vesicle transport, and unfolded protein response (Supplementary Table 6).[89–92] We found secreted *MUC2* and transmembrane *MUC13* expressed across organs and colon-enriched *MUC1*, *MUC4*, and *MUC5B* (Figure 10*B* and *C*). Although GCs are considered the major intestinal mucus producers, we also mapped glycocalyx-forming transmembrane mucins, which protect against pathogenic bacteria,[93,94] in AEs and ACCs (Figure 10*D*).

GCs commonly are considered homogenous, however, GCs in the mouse colon recently were separated into functionally distinct groups, with intercrypt GCs (icGCs) producing more permeable mucus than crypt-resident GCs.[95] Human colonic secretory progenitors and GCs subclustered into similar groups corresponding with differentiation status and marked by genes defined in mouse GC heterogeneity[95] (Figure 10*E*–*H*). Distinct icGCs on the colon surface were visualized using immunofluorescence, with RAB27A localized to the surface GC cells (Figure 10*I*). Some mucus secretion genes (*MUC2*, *ZG16*) were expressed highest in icGCs, consistent with icGCs constitutively secreting mucus,[96] and this was supported by higher mucin 2 (MUC2) seen in surface GCs via immunofluorescence (Figure 10*I* and *K*). Notably, crypt-resident GCs and icGCs expressed different mucin genes (Figure 10*C*), as verified with immunofluorescence showing crypt base–specific mucin 5b (MUC5B) protein expression (Figure 10*K*) and consistent with distinct mucus production in human beings shown via lectin staining.[95] Similar SI subclusters were observed with less obvious mucin differences (Figure 11). The physiological significance of this human GC heterogeneity necessitates further functional studies.

Enteroendocrine Cells

EECs secrete hormones to communicate throughout the body. EEC hormone profiles have been characterized at the single-cell level in mice, using EEC reporters to enrich for this rare lineage.[97,98] However, transcriptomic differences exist between mouse and human EECs.[97,99] Human organoids with an EEC reporter yielded sufficient EECs for scRNAseq analysis, although potential differences from primary EECs are unclear.[97] Although several human scRNAseq studies include EECs,[4–6,9,10] our 154 EECs represent a large and informative scRNAseq data set of primary human EECs.

Regional expression of hormones and other signaling machinery in EECs was surveyed (Figure 12*A*–*C*). An early study that immunostained regional biopsy specimens found SI-segregated Cholecystokinin (CCK), gastrin (GAST), gastric inhibitory polypeptide (GIP), neurotensin (NTS), motilin (MLN), and secretin (SCT).[100] Our data confirm this bias but additionally detected low levels of *CCK*, *NTS*, *MLN*, and *SCT* in colonic EECs, suggesting higher sensitivity of scRNAseq. Colonic *NTS* and *CCK* expression also was absent in a study analyzing region-unspecified colon,[6] emphasizing the importance of analyzing all colon regions. Fatty acid receptors *FFAR1* and *FFAR2* were enriched in SI EECs, with *FFAR4* specific to colon (Figure 12*C*). EECs also express several hormone receptors, indicating crosstalk among EECs. Novel gut–brain crosstalk recently was described, with murine EECs forming synapses with the vagus nerve.[101–103] Thirty-one DEGs from SI and colon EECs are in the GOCC_Presynapse list (Figure 12*D*) and 33.7% of genes in the GOCC_Presynapse list expressed highest in EECs (Figure 12*E*), suggesting a human equivalent of these mouse EECs, termed *neuropods*.[102] These patterns describe EEC crosstalk within the gut and between the gut and brain, further illuminating newly appreciated functional roles of EECs.

EECs are classified into subtypes by hormone expression.[104,105] A regional breakdown of individual EECs was constructed to visualize EEC subtypes (Figure 12*F*). Enterochromaffin cells appear in each region, and ileal L cells were undetected. Multiple EECs express 8–10 hormones, expanding on studies identifying polyhormonal EECs.[106,107] *GAST* and *GIP* largely segregated from duodenal L cells yet overlapped in jejunum. We noted rare *NPY* expression in MLN^+ and $GHRL^+$ EECs in jejunum and AC. Future studies combining our EECs with additional regional data sets hopefully will improve our understanding of EEC subclusters.

Absorptive Enterocytes and Colonocytes

AEs and ACCs perform nearly all intestinal absorption.[108] Three AE Leiden clusters and 2 ACC clusters were consistent with increasing maturity, reflecting other reports,[4,9,33] and 1 cluster largely from donor 3 ileum (AE2) separated from other AEs (Figures 1*C* and 13*B*). A DEG signature was defined by comparing DEGs from all AEs and all ACCs. Surprisingly, only 5 DEGs were shared across SI and colonic absorptive populations (Figure 13*A*), indicating stark organ differences. AE2s expressed mature AE markers

Figure 7. (***See previous page***). **Paneth cells.** (*A*) Heatmap of DEGs in PCs vs other lineages (red: classic markers). (*B*) Dotplot showing lysozyme mRNA expression across FAE, BEST4, Paneth, and tuft cell lineages. (*C*) Dotplot showing expression of PC, goblet, and $BEST4^+$ cell classic markers across the PC, goblet, and $BEST4^+$ cell clusters. (*D*) Dotplot showing growth factors shown to be expressed in murine PCs in previous literature across human SI lineages. (*E*) Dotplot showing all members of major intestinal growth factor families that show detectable expression in PCs across SI lineages. (*F*) Heatmap showing PC (*top*) and ISC markers (*bottom*) across all SI ISCs (*left*) and PCs (*right*). (*G*) Immunofluorescence staining for LYZ protein (magenta), in situ hybridization showing *SMOC2* mRNA (white), and nuclei (blue) in a human ileum crypt base. Maximum projection of eight 0.5-μm optical slices. *Scale bar*: 20 μm. (*H*) Dotplot showing expression of all Frizzled family receptors across SI lineages. (*I*) Dotplot showing the 10 highest-expressed antimicrobial peptides across SI lineages.

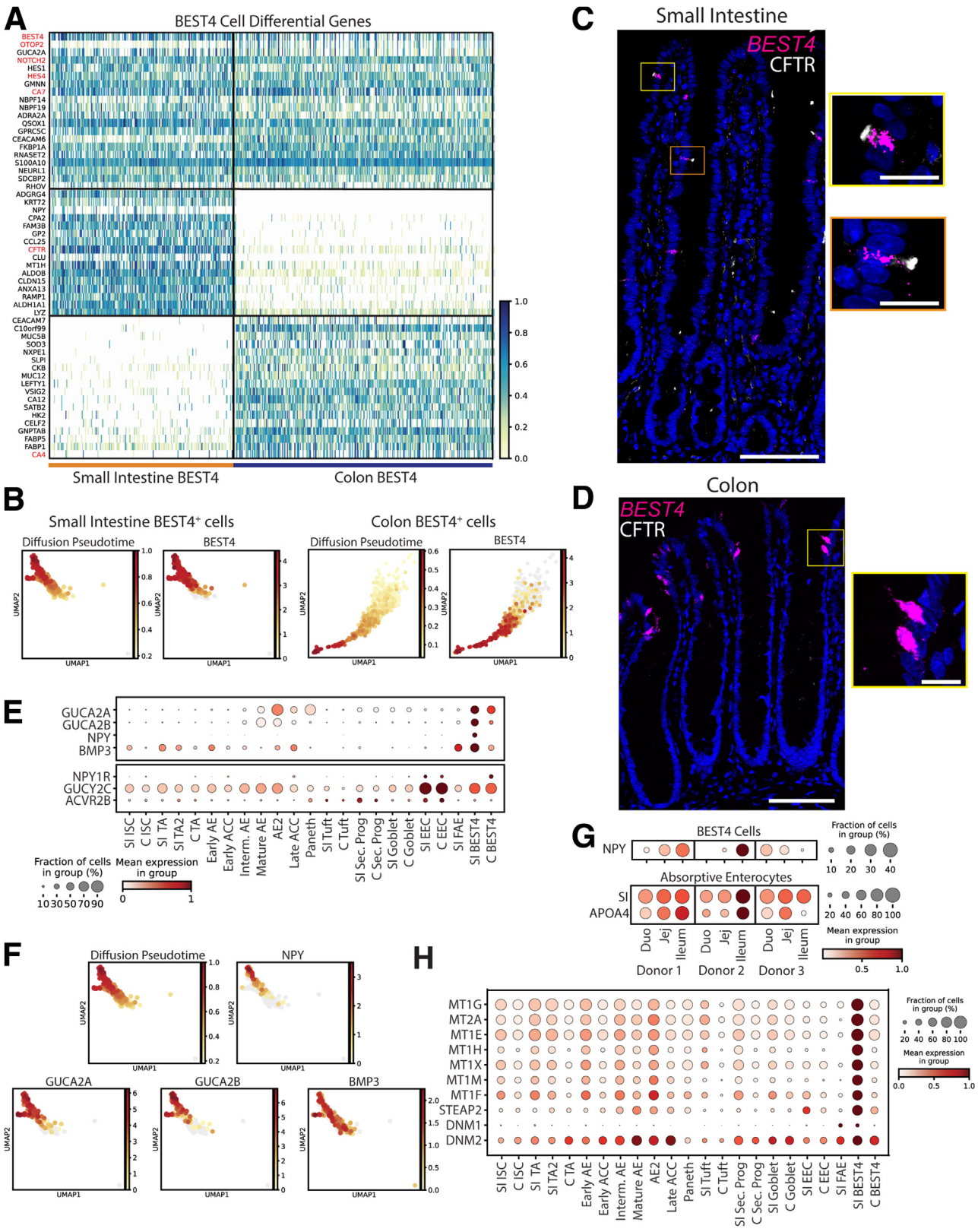

Figure 8. BEST4$^+$ cells. (*A*) Heatmap of DEGs in BEST4$^+$ cells vs other lineages (*top*; red: classic markers), SI vs colon BEST4$^+$ cells (*middle*), colon vs SI BEST4$^+$ cells (*bottom*). (*B*) UMAPs showing all SI (*left*) and colon (*right*) BEST4$^+$ cells colored according to predicted diffusion pseudotime or expression of *BEST4* mRNA. (*C* and *D*) In situ hybridization showing *BEST4* mRNA (magenta), immunofluorescence staining CFTR protein (white), and nuclei (blue) in human (*C*) jejunum and (*D*) colon. *Scale bars*: 100 μm; 20 μm (*zoomed panels*). (*E*) Dotplot showing secreted genes (*top*) and their receptors (*bottom*) across lineages. (*F*) UMAPs of BEST4$^+$ cells showing predicted diffusion pseudotime and expression of secreted peptides. (*G*) Expression of *NPY*, *SI*, and *APOA1* across regions for each donor. (*H*) Dotplot showing genes involved in metal binding and endocytosis across lineages. UMAP, Uniform Manifold Approximation and Projection. CFTR, Cystic Fibrosis Transmembrane Conductance Regulator; GUCA2, Guanylate Cyclase Activator 2A; NPY, Neuropeptide Y.

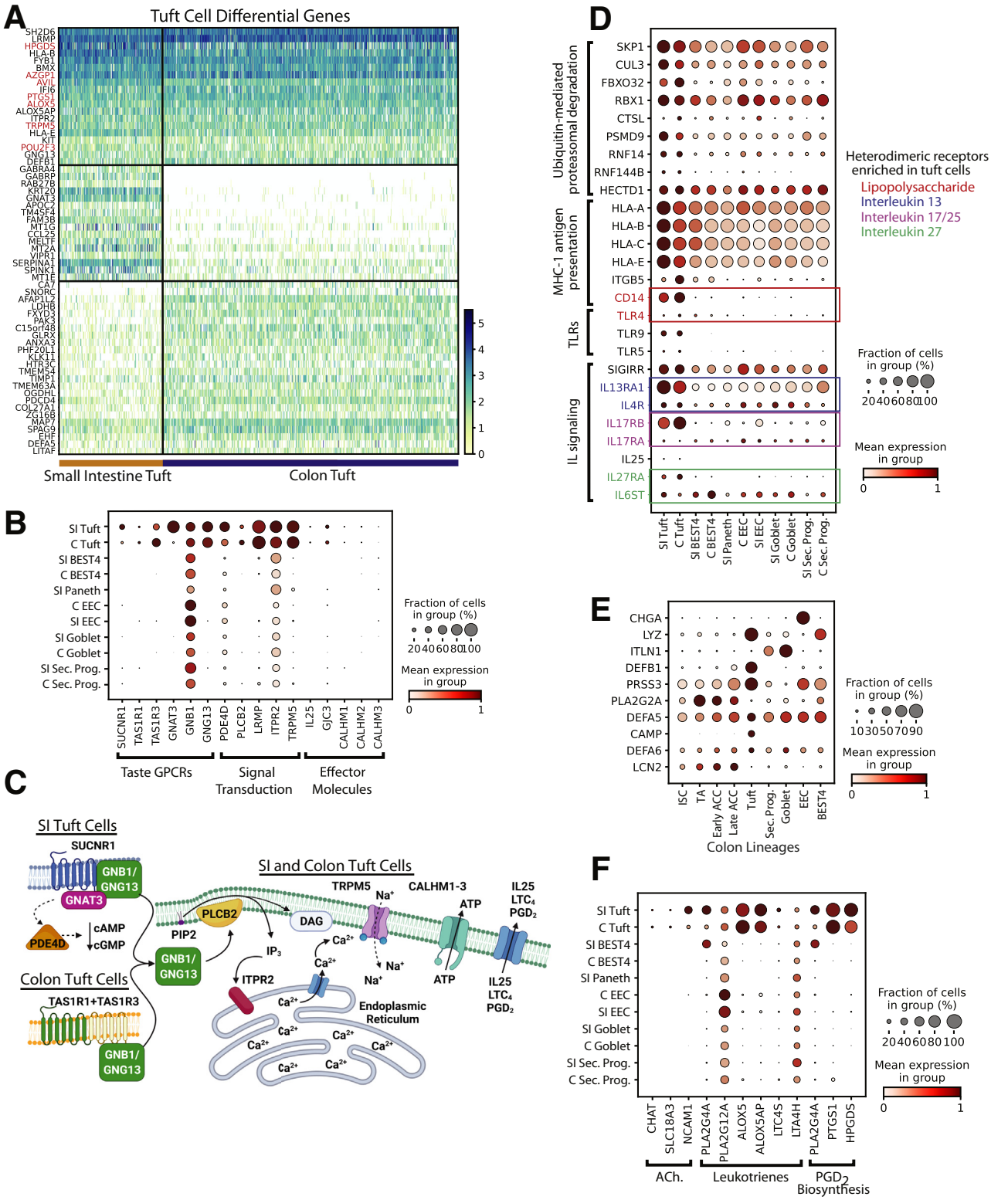

Figure 9. Tuft cells. (*A*) Heatmap of DEGs in tuft cells vs other lineages (*top*; red: classic markers), SI vs colon tuft cells (*middle*), and colon vs SI tuft cells (*bottom*). (*B*) Dotplot showing tuft cell enrichment of genes specific to taste signal transduction. (*C*) Organ-specific signal transduction in SI vs colon tuft cells. (*D*) Dotplot showing tuft cell–enriched genes enabling interactions with innate and adaptive immune system. (*E*) Dotplot showing 10 highest-expressed antimicrobial peptides across colon lineages. (*F*) Dotplot showing tuft cell–specific genes for producing acetylcholine, eicosanoids, and prostaglandins. Schematics in panel *C* were created with BioRender.com. C, Colon; GPCR, G-protein Coupled Receptor; MHC, major histocompatibility complex; TLR, Toll-like receptor.

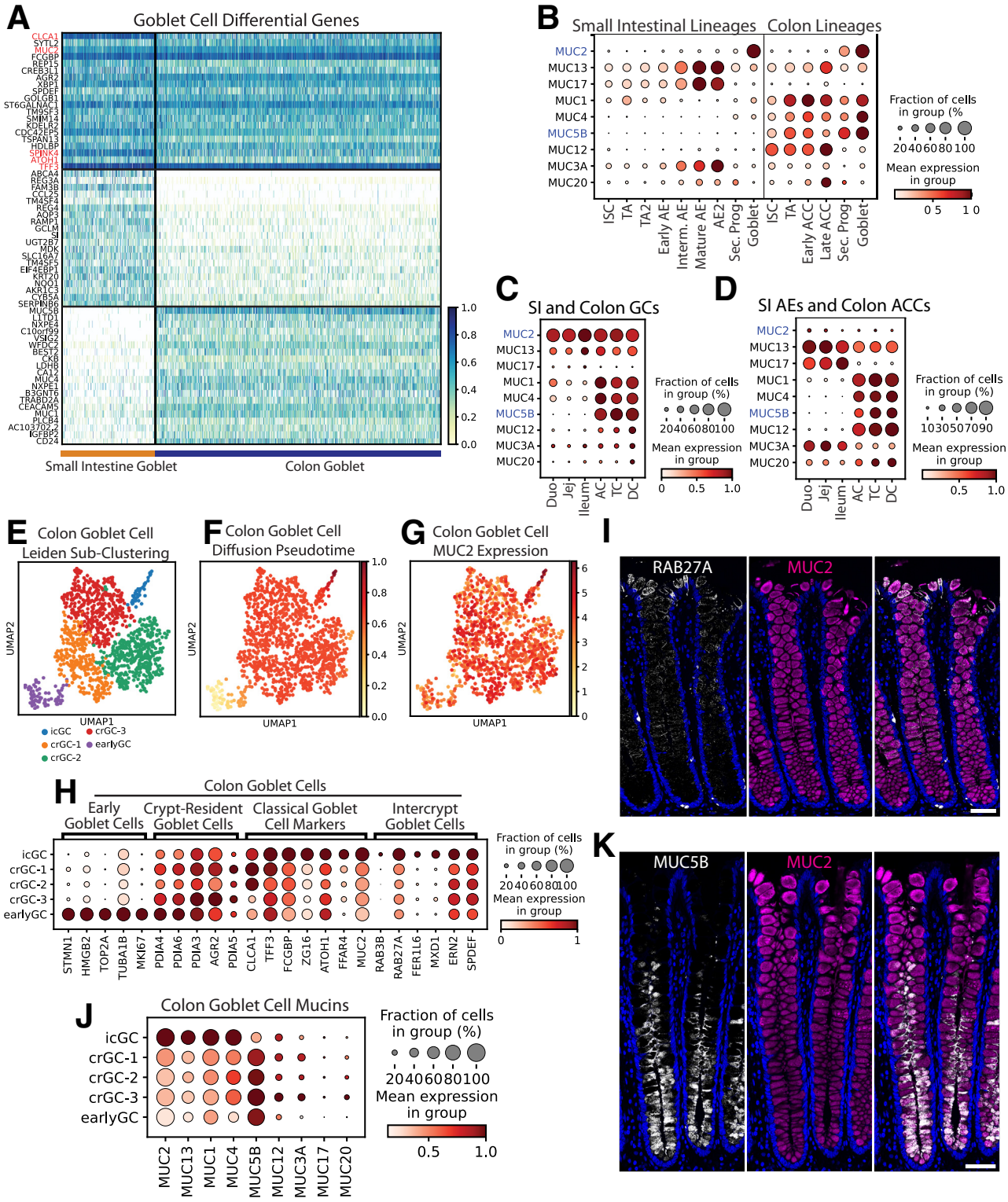

Figure 10. Goblet cells. (*A*) Heatmap of DEGs in GCs vs other lineages (*top*; red: classic markers), SI vs colon GCs (*middle*), and colon vs SI GCs (*bottom*). (*B*) Dotplot showing expression of the 9 highest-expressed mucins across GCs and proliferative and absorptive lineages of the SI and colon (blue: gel-forming mucins). (*C*) Dotplot showing the 9 highest-expressed mucins across GCs by region. (*D*) Dotplot showing expression of the 9 highest-expressed mucins in all absorptive enterocytes and colonocytes by intestinal region. (*E*) Leiden subclustering of colon GCs. (*F*) Diffusion pseudotime of colon GCs. (*G*) UMAP of *MUC2* expression in colon GCs. (*H*) Dotplot showing markers of murine GC subpopulations in the human colon GC subclusters defined in panel *E*. (*I*) Immunofluorescence staining for protein expression of RAB27A (white), MUC2 (magenta), and nuclei (blue) in human colon (2-μm optical slice). (*J*) Dotplot showing expression of mucins in colonic icGCs, crypt-resident goblet cells (crGCs), and early goblet cells. (*K*) Immunofluorescence staining for protein expression of MUC5B (white), MUC2 (magenta), and nuclei (blue) in human colon (2-μm optical slice). *Scale bars*: 50 μm. UMAP, Uniform Manifold Approximation and Projection; Duo, Duodenum; Jej, Jejunum.

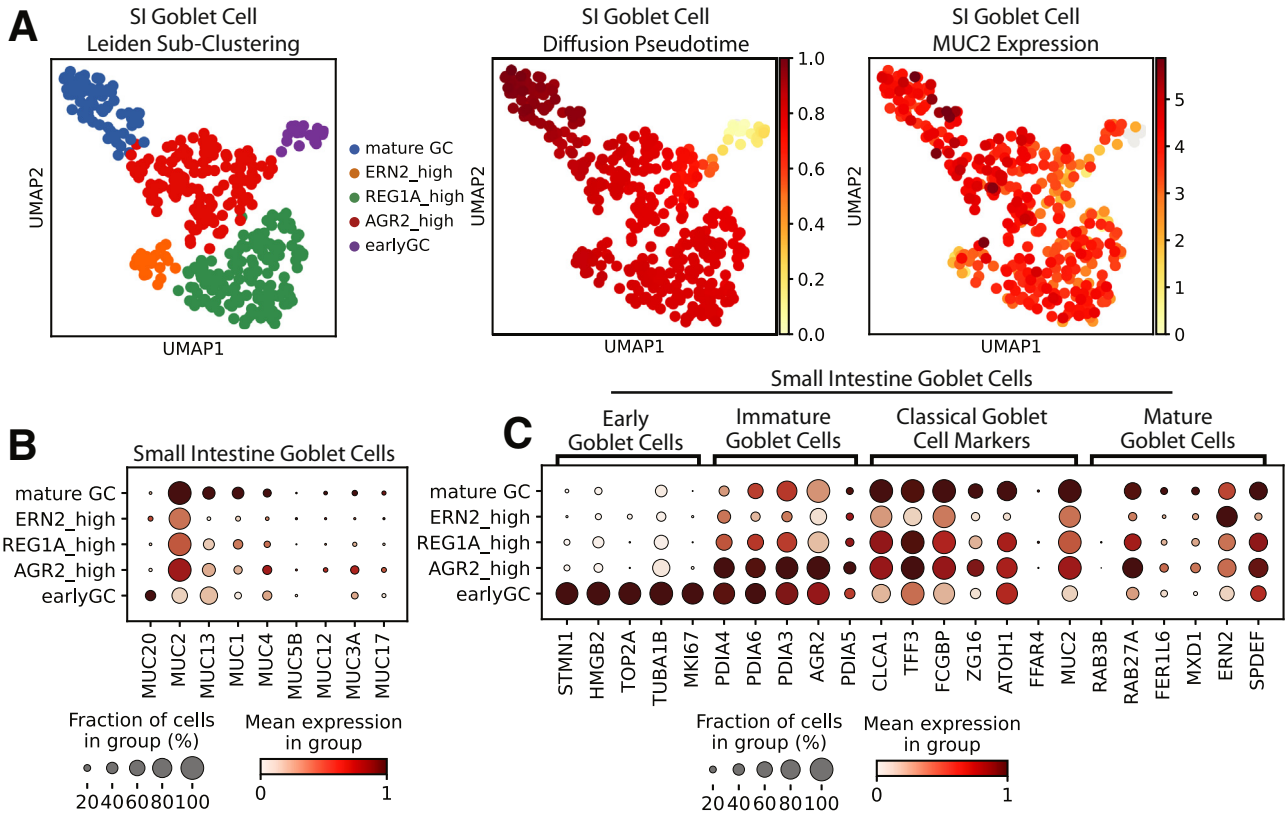

Figure 11. SI goblet cell subclustering. (*A*) *Left*: Leiden subclustering of SI goblet cells, with subclusters named according to genes with high expression. *Middle*: UMAP of SI goblet cells marked by diffusion pseudotime. *Right*: UMAP of SI goblet cells marked by *MUC2* expression. (*B*) Dotplot showing expression of mucins in SI GC subpopulations. (*C*) Dotplot showing expression of mouse-implicated markers of GC subpopulations in human SI GC subclusters. UMAP, Uniform Manifold Approximation and Projection.

(Figure 13*B*) alongside bile acid absorption genes[109] (Figure 13*C*). It is unclear why ileal AEs of donor 3 clustered separately. Possible explanatory donor-specific demographics include donor 3 having the lowest body mass index, being the only African American, and the only donor with type II diabetes. Meal timings across donors also might induce unique expression patterns, as described for certain genes.[56,57]

Macronutrient and micronutrient handling was mapped across all AEs and ACCs (Figure 13*D*). Most fatty acid, glucose, and cholesterol transporters were SI-enriched, with regional data showing increasing expression from duodenum through ileum for most genes (Figure 13*D*). Digestive enzymes showed ileal enrichment, except for the duodenum-specific serine protease *TMPRSS15*/enteropeptidase.[110] Ion transporters showed the most regional differences, with *SLC25A3* and *SLC4A4* spanning all regions, colon-enriched *SLC26A2*, and SI-enriched *SLC9A3R1*. Finally, *SCNN1* sodium transporter subunits were colon-enriched, possibly regulating colonic water uptake. This regional map expands upon previous organ-level analyses, emphasizing the importance of the ileum in digestion.

Intestinal barrier function, largely conferred by cell-junction proteins, is essential for well-regulated absorption and antimicrobial defense.[111] Regional mapping of the 20 highest-expressed cell junction genes (Figure 13*E*) showed equal expression of many cell-junction genes across AEs and ACCs, while others showed regional enrichment. Claudins (*CLDN*) are primary determinants of tight junction barrier function and epithelial integrity.[108,111] *CLDN1* and *CLDN15* were SI-enriched, and *CLDN3*, *CLDN4*, and *CLDN7* were highest in TC. Notably, no cell junction genes were expressed highest in DC. Ulcerative colitis often originates in the distal large intestine, raising the possibility that higher junction protein expression in AC and TC might protect against certain inflammatory conditions.[112–114]

Aquaporin proteins (AQPs) are the major intestinal transcellular water transporters.[115] We confirm a previous report showing increased *AQP3*, *AQP7*, and *AQP11* in ileum vs colon and colon-enriched *AQP8* (Figure 13*F*); however, we found *AQP1* widely expressed.[6] Aquaglyceroporin (*AQP3*, *AQP7*, *AQP10*) expression is highest in mature AEs (Figure 13*G*) and increases from duodenum to ileum alongside lipid metabolism genes (Figure 13*D* and *F*). This suggests AQP-mediated glycerol transfer functions in AE triglyceride processing. We note unappreciated *AQP1* specificity in ISCs and TA cells and uniquely restricted *AQP8* expression in the most mature late ACCs in the AC (Figure 13*H*). These distinct differences suggest specific physiological roles that should be functionally investigated.

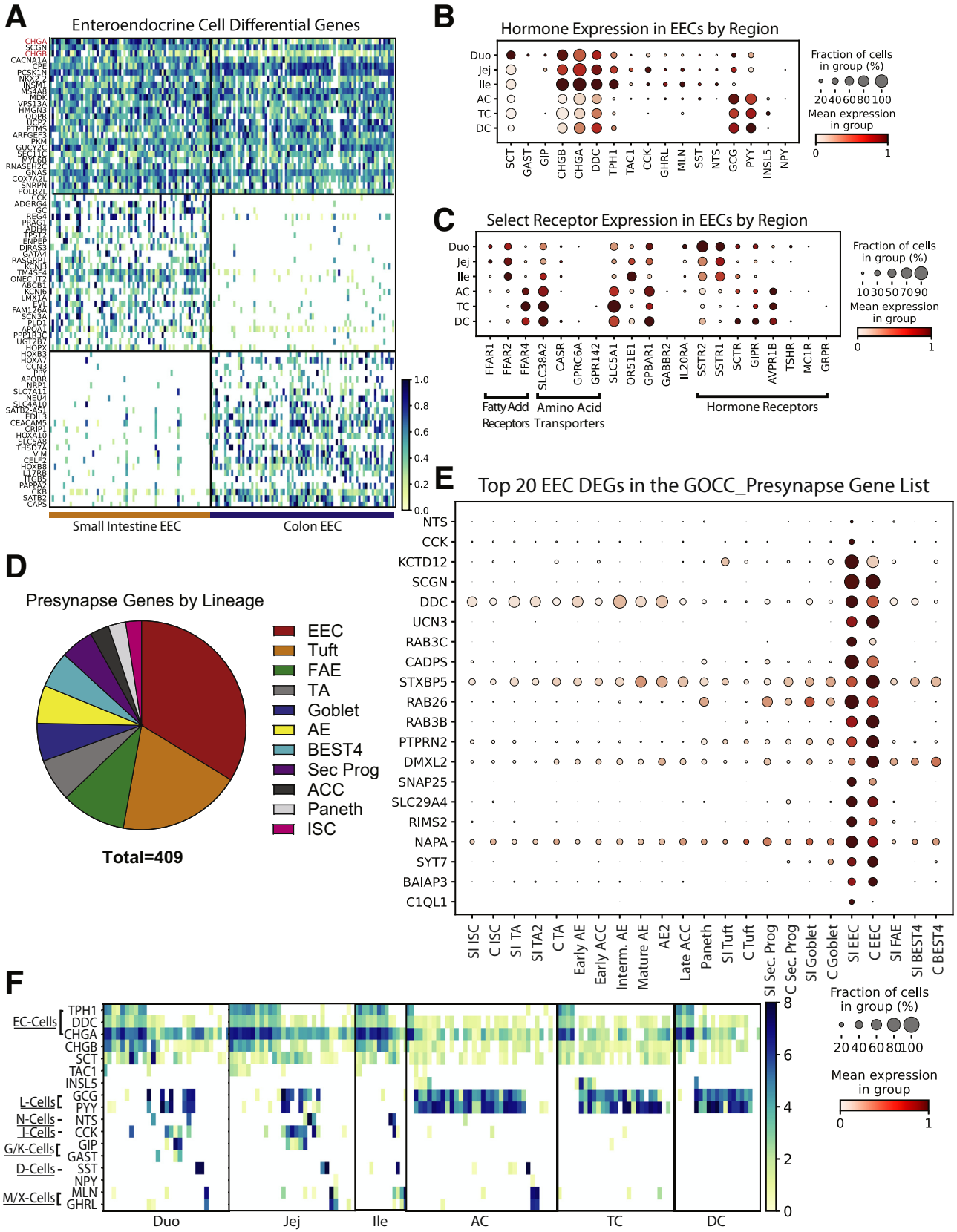

Figure 12. Enteroendocrine cells. (*A*) Heatmap of DEGs in EECs vs other lineages (*top*, red: classic markers), SI vs colon EECs (*middle*), and colon vs SI EECs (*bottom*). (*B*) Dotplot of EEC regional hormone gene expression. (*C*) Dotplot of EEC expression of select receptors by region. (*D*) Dotplot showing expression of DEGs of SI or colon EECs that are present in the GOCC_Presynapse gene list. (*E*) Pie chart of all genes within the GOCC_Presynapse gene list shown by lineage in which they have the highest expression (SI and colon lineages are combined when applicable). (*F*) Heatmap showing hormone expression in each individual EEC. Duo, Duodenum; G/K, G-cells/K-cells; Ile, Ileum; Jej, Jejunum; M/X, M-cells/X-cellsD.

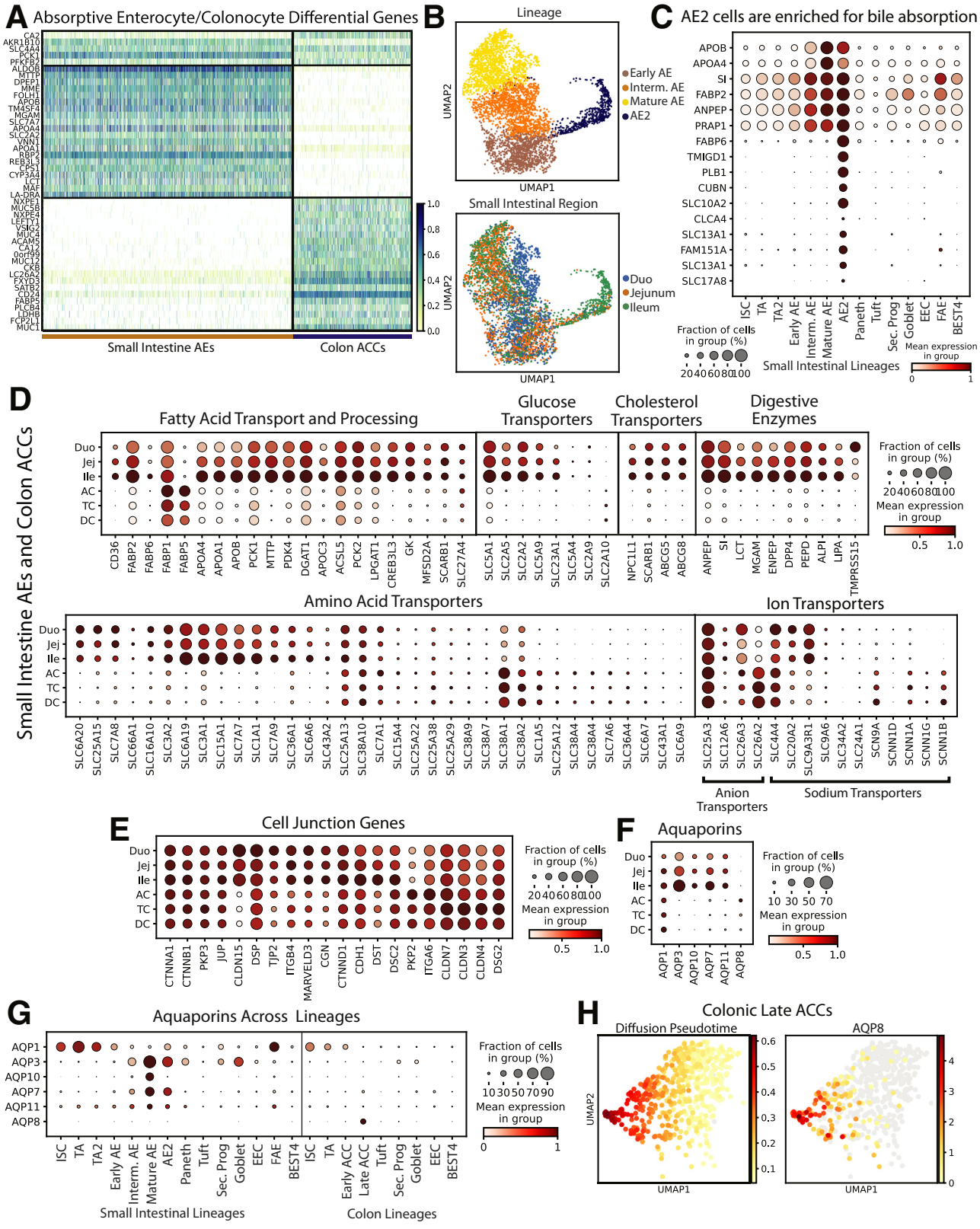

Figure 13. Absorptive cells. (*A*) Heatmap of DEGs in absorptive cells vs other lineages (*top*), AEs vs ACCs (*middle*), and ACCs vs SI AEs (*bottom*). (*B*) UMAPs showing the AE2 Leiden cluster (*top*) and cells by region (*bottom*). (*C*) Dotplot of classic mature AE markers and top 10 DEGs for AE2 cluster. (*D*) Dotplots showing regional expression of genes involved in digestion and absorption in all AEs and ACCs. (*E*) Dotplots showing the 20 highest-expressed cell junction genes in AEs and ACCs by region. (*F*) Dotplots showing regional aquaporin expression in AEs and ACCs. (*G*) Dotplot showing aquaporin expression across lineages. (*H*) UMAPs of late ACCs showing predicted diffusion pseudotime (*left*) and *AQP8* expression (*right*). UMAP, Uniform Manifold Approximation and Projection; Duo, Duodenum; Ile, Ileum; Jej, Jejunum.

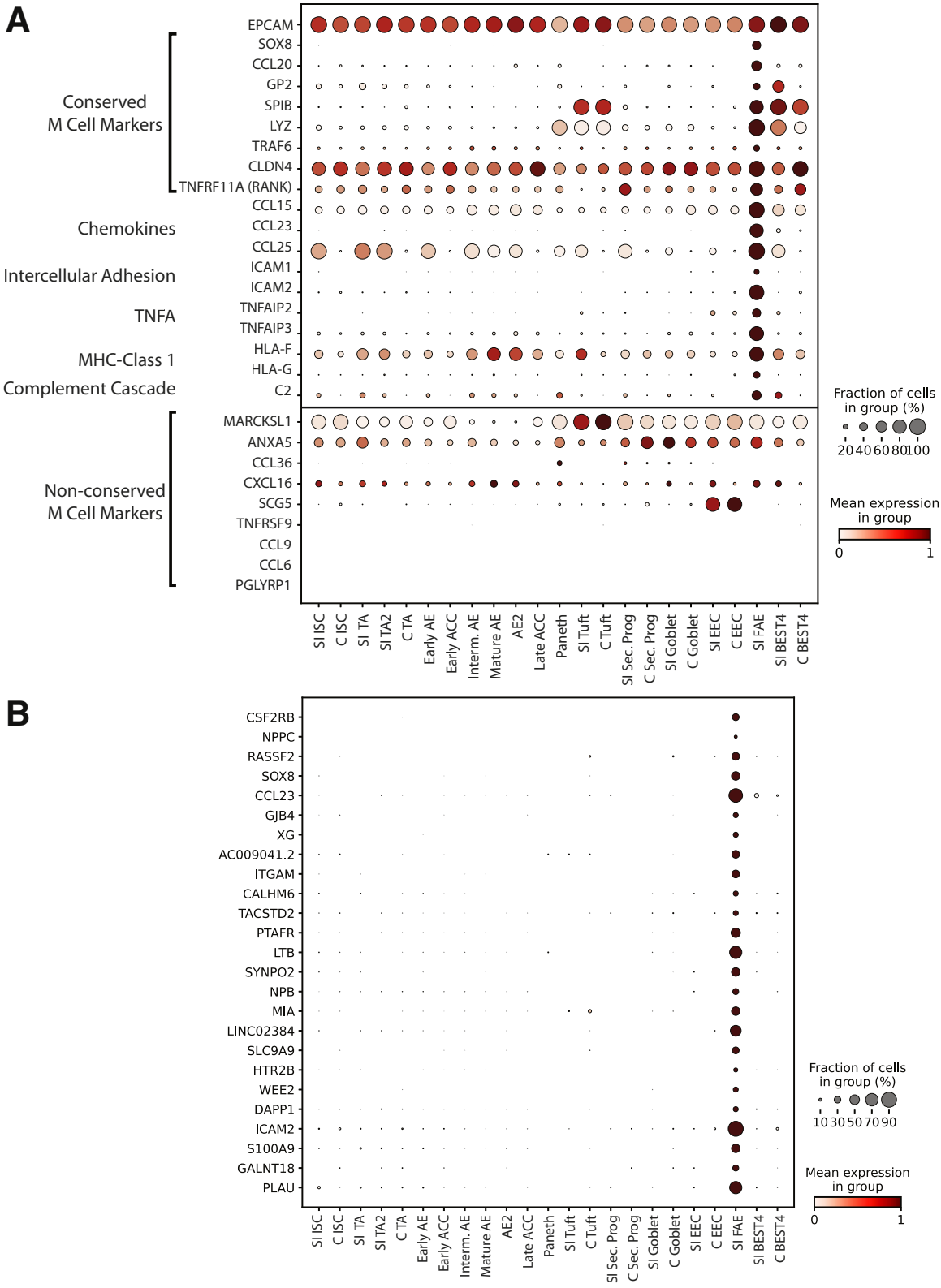

Figure 14. Follicle-associated epithelium. (*A*) *Top*: Dotplot showing expression of EPCAM and conserved M-cell markers and other genes known to interact with the immune system across lineages. *Bottom*: Genes implicated in mouse M cells that are not specific to human FAE. (*B*) Dotplot showing expression of the top 20 FAE DEGs across lineages. EPCAM, Epithelial Cell Adhesion Molecule; C, Colon; MHC, major histocompatibility complex; TNFA, Tumor Necrosis Factor Alpha.

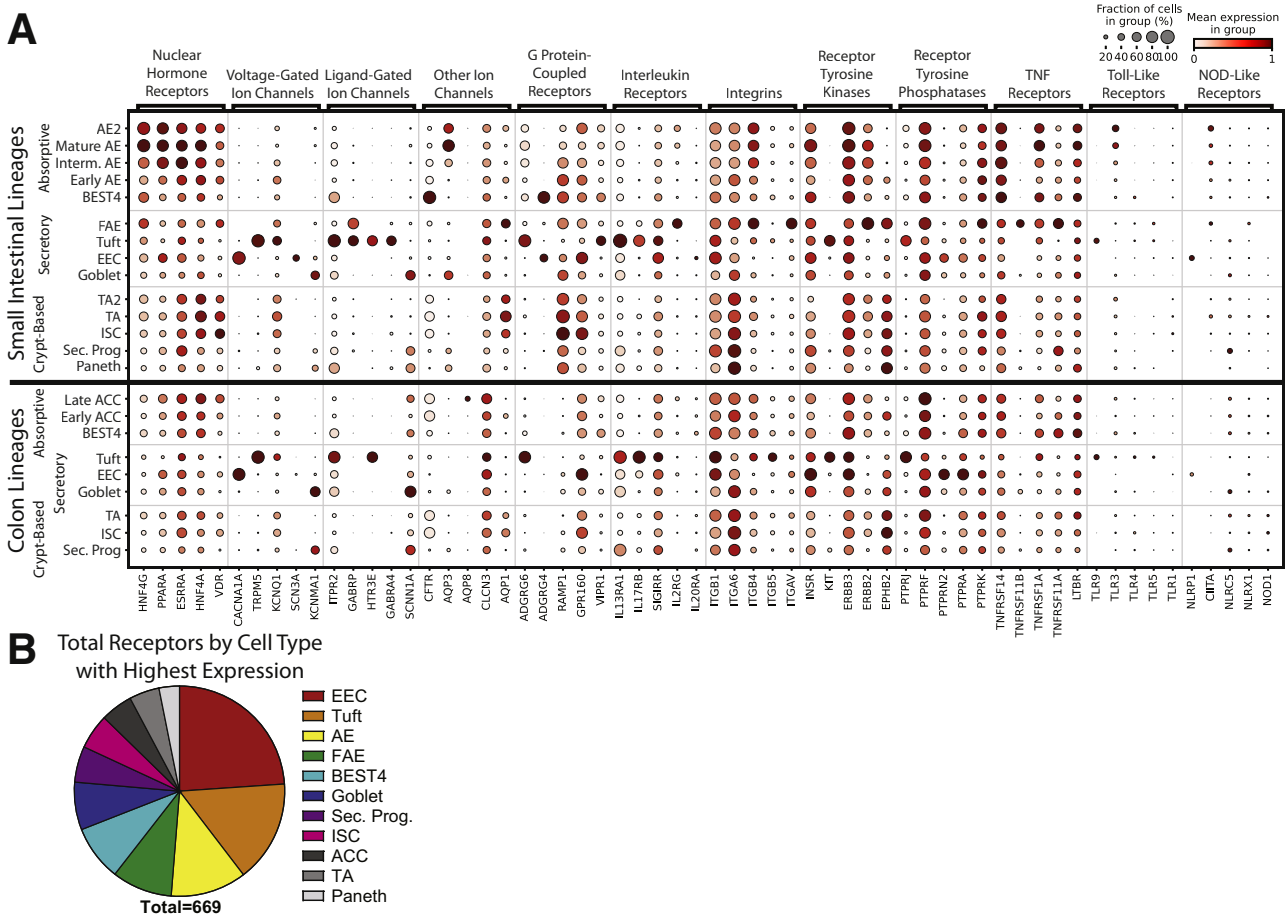

Figure 15. Extrinsic receptors and drug targets. (*A*) Dotplot showing expression of the 5 highest-expressing members of each major receptor family by lineage. *Top*: Small intestinal lineages. *Bottom*: Colonic lineages. (*B*) Pie chart showing receptor genes expressed in the intestinal epithelium by lineage with the highest expression. NOD, Nucleotide-binding Oligomerization Domain Sec. Prog., Secretory Progenitor; TNF, tumor necrosis factor.

Follicle-Associated Epithelium

Rare FAE cells reside in small puncta throughout the intestines.[116] FAE includes microfold (M) cells, which transport luminal antigens to resident immune cells.[117] M cells have been explored almost exclusively in mice[118–120] or using directed differentiation in vitro,[121] with only 1 scRNAseq study isolating healthy human M cells.[10] Our data set included a 19-cell cluster from a single donor (donor 2) enriched for microfold cell (M-cell) markers[122–124] and immune crosstalk genes while still expressing Epithelial Cell Adhesion Molecule (EPCAM) (Figure 14*A*). We defined 145 DEGs (Supplementary Table 1), finding many FAE-unique genes (Figure 14). Pathway enrichment analysis implicated these DEGs in immune cell interactions, verifying expected M-cell function (Supplementary Table 7). Several murine M-cell–specific markers,[117,123,125] were either widely expressed or absent (Figure 14), suggesting species functional differences. Because these data arise from a small set of cells from a single donor, future studies are necessary to fully define these cells, possibly through enriching for FAE using recently described methods.[116]

Receptors/Drugs

We finished by designing 2 approaches showing how to find associations between lineages, receptors, and drug targets. Major receptor families were surveyed across lineages and classified as high-, intermediate-, or low-expressing (Supplementary File 1, Supplementary Table 8). The 5 highest-expressing genes per family were grouped across lineages (Figure 15*A*). Several patterns appeared from these 60 receptors: 20 receptors were highest-expressed in tuft cells, 11 in EECs, 10 in AE/ACC, and 9 in FAE; 12 villi-enriched vs 3 crypt-enriched; 4 SI-enriched vs 0 colon-enriched; and many uniquely marked individual lineages (12 in tuft cells, 3 in EECs, and so forth), showing potential ways to target regions and lineages.

To test the novelty of these observations, we reviewed literature regarding the 12 receptors found to be unique to tuft cells. We found direct literature connections to human or mouse intestinal tuft cells for only 5 of 12 receptors (*TRPM5*, *ITPR2*, *HTR3E*, *IL13RA1*, *IL17RB*), with no connection found for 7 receptors (*GABRA4*, *ADGRG6/GPR126*, *SIGIRR*, *ITGB5*, *KIT*, *PTPRJ*, *TLR9*). These 7 unappreciated

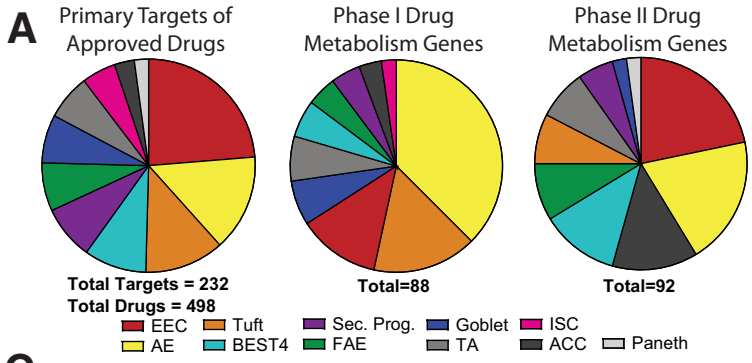

B

Drug	Function	Target
Tacrolimus	Immunosuppressant	FKBP1A
Mycophenolate Mofetil	Immunosuppressant	IMPDH1, IMPDH2
Tofacitinib	JAK Inhibitor	JAK1, JAK2, JAK3
Methotrexate	Immunosuppressant	DHFR
Prednisolone	Corticosteroid	NR3C1
Prednisone	Corticosteroid	NR3C1
Natalizumab	Immune Cell Blocker	ITGA4
Vedolizumab	Anti-Inflammatory	ITGA4

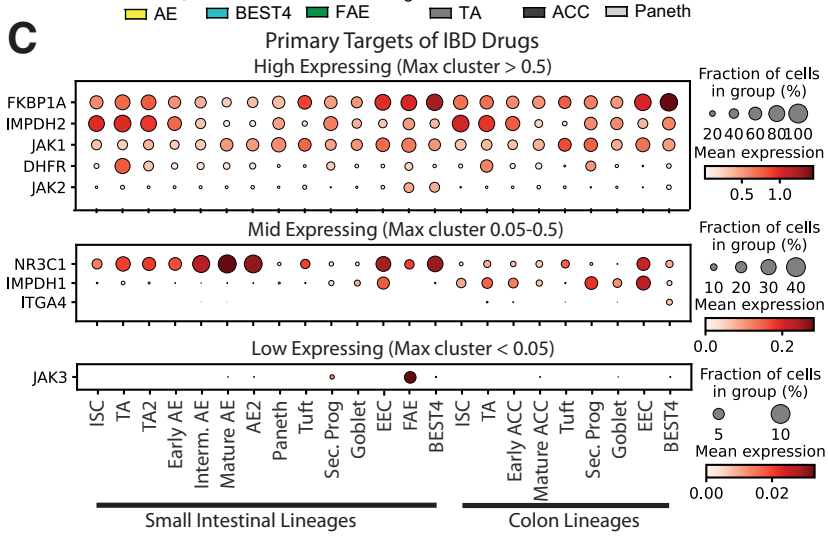

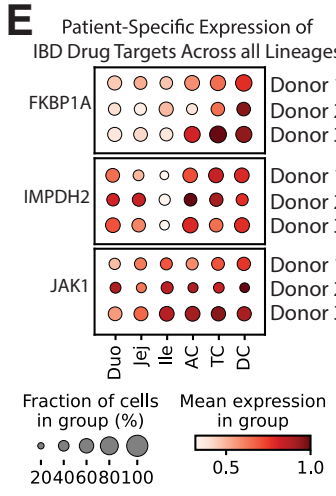

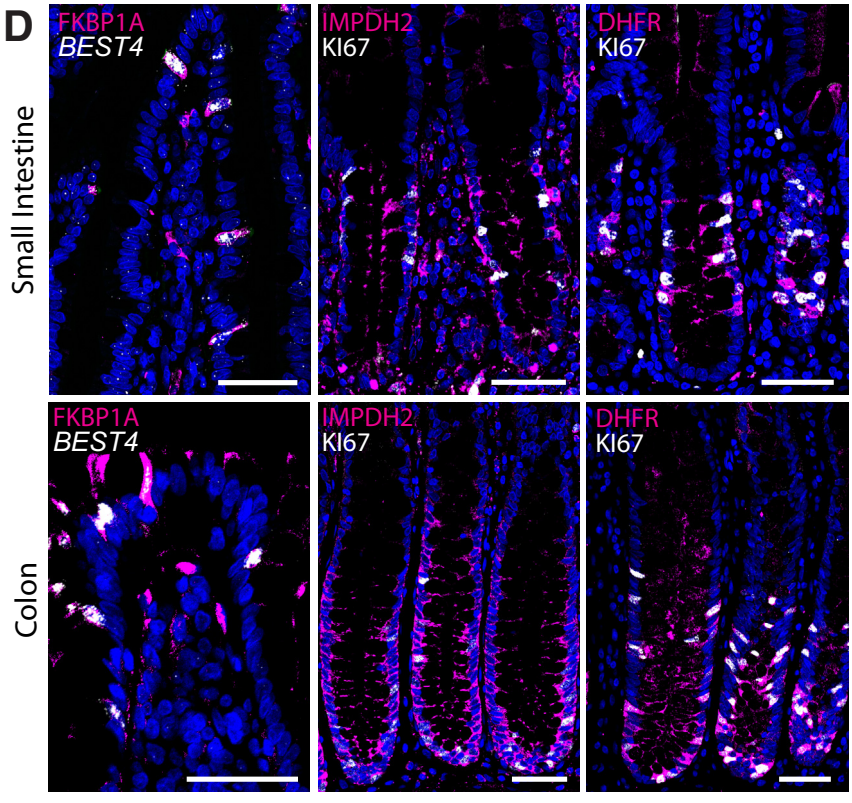

lineage-specific receptors arose from analyzing just 60 receptors in 1 lineage, and our full data set included 669 total receptors (Figure 15*B*, Supplementary File 1). This receptor atlas across lineages, organs, regions, and donors provides a powerful foundation to explore how extrinsic signals from local microenvironments, dietary and microbial influences, and pharmaceuticals may affect intestinal epithelial lineages.

We next explored how pharmacologic agents might directly affect the intestinal epithelium. Few drugs deliberately target the intestinal epithelium[126–129] and common GI side effects often are unexplained at the cell-lineage level.[130] We found 498 Food and Drug Administration–approved drugs had 232 primary gene targets expressed in our gut epithelial data set (Figure 16*A*, Supplementary Table 9). Beyond primary targets in the gut epithelium, lineages express many enzymes that can functionalize drugs through metabolism.[127–129] We show gene expression for phase I and phase II drug metabolism enzymes by lineage with the highest expression in the intestinal epithelium (Figure 16*A*) and quantified gene expression by lineage and region (Supplementary Table 10). We found *CES2*, which metabolizes the cancer drug irinotecan into biologically active SN-38,[131] to be the highest-expressed phase I metabolism gene in the SI, with AE enrichment. Interestingly, *UGT1A1*, the phase II enzyme that inactivates SN-38,[132] has low gut epithelial expression (Supplementary Table 10). This suggests that irinotecan may experience prolonged activation in the gut, advancing the idea that orally administered irinotecan might be effective against intestinal cancers.[133–135] Our easily searchable data set quantifies the expression of genes important for intestinal metabolism of endobiotics, environmental toxicants, and pharmaceuticals.

As an example of a disease-focused approach, we evaluated primary gene targets of drugs prescribed for inflammatory bowel disease (IBD). Most IBD drugs are anti-inflammatory or immunomodulatory, so primary targets often are not expressed in the intestinal epithelium, yet our database shows 9 primary gene targets of 8 IBD drugs have epithelial expression (Figure 16*B*). We mapped epithelial expression of their primary target genes to locate potential off-target effects (Figure 16*C*). We found high *FKBP1A*, a tacrolimus (Prograf, Astellas Pharma Inc., Tokyo, Japan) target, in the little-understood BEST4^{+} cells. Mycophenolate mofetil (CellCept, Genentech, South San fransisco, CA) targets *IMPDH2* and *IMPDH1* were expressed in proliferative crypt populations and EECs, respectively. The methotrexate target *DHFR* was highest in TA and progenitor cells, while the tofacitinib (Xeljanz, Pfizer, New York, NY) target *JAK1* had broader expression. Because functional protein expression is not always found in the same cells as mRNA translation, especially given the quick cellular turnover of the intestine,[136] we stained for protein expression of the top 3 highest expressed gene targets that appear enriched in specific cell types: FKBP1A, IMPDH2, and DHFR. We found all 3 proteins enriched in the lineages implicated by our transcriptional data (Figure 16*D*), highlighting the usefulness of our data set for predicting drug targets. These drugs can be orally administered and primary targets in the epithelium could explain common GI side effects.[137–139] This small subset of drug targets highlights a spectrum of potential unintended epithelial effects on ISC/TA renewal, EEC hormonal regulation of appetite and gut motility, and unknown effects from other lineages.

Personalized precision medicine is an emerging field motivating new technologies.[140] We used our drug-target atlas to assess regional variability of tacrolimus, mycophenolate mofetil, and tofacitinib target genes, *FKBP1A*, *IMPDH2*, and *JAK1*, across individual donors to inform potential patient-dependent effects (Figure 16*E*). Higher colonic expression of all 3 targets suggests that patients may experience colon-specific off-target effects. Comparing donors potentially hints at susceptibility to drug side effects, with donors 2 and 3 generally expressing target genes higher than donor 1. Although 3 donors are insufficient for statistically significant conclusions, we provide a framework to generate observations to inform larger studies. We hope our lineage-, regional-, and donor-specific data on primary drug targets will aid gastroenterology and pharmacology to better understand potential intestinal drug effects.

Discussion

In this study, we provide a comprehensive cell-level transcriptomic view of the SI and colon epithelium with regional resolution across multiple human beings. Our analyses independently confirm and advance prior studies, define important differences between mouse and human beings, and highlight how lineages vary along the proximal–distal axis. We include easy-to-search tables for DEGs, receptors, and drug targets that can be investigated by most investigators and trainees. Overall, our database provides a foundation for understanding individual contributions of diverse epithelial cells across the length of the human intestine and colon to maintain physiologic function.

Figure 16. (***See previous page***). **Drug targets.** (*A*) Pie charts of primary targets of all approved drugs (*left*) and all phase I (*center*) and phase II (*right*) drug metabolism genes expressed in the intestinal epithelium shown by lineage with highest expression. (*B*) Primary targets of drugs used to treat IBD found to have expression in the intestinal epithelium. (*C*) Dotplots showing expression of primary targets of drugs used to treat IBD by lineage split into high-, middle-, and low-expressing tables for better visualization. Note scaling changes between tables. (*D*) *Left*: In situ hybridization showing *BEST4* RNA (white) and immunofluorescence staining for FKBP1A protein (magenta) and nuclei (blue) in human jejunum (*top*) and colon (*bottom*). *Center*: Immunofluorescence staining for IMPDH2 protein (magenta), KI67 (white), and nuclei (blue) in human jejunum (*top*) and colon (*bottom*). *Right*: Immunofluorescence staining for DHFR protein (magenta), KI67 (white), and nuclei (blue) in human jejunum (*top*) and colon (*bottom*). Optical slice was 2 μm for all. *Scale bars*: 50 μm. (*E*) Dotplot showing expression of the top 3 highest-expressed targets of IBD drugs in the intestinal epithelium across regions and split by donor. FKBP1A, FKBP Prolyl Isomerase 1A; IMPDH2, Inosine Monophosphate Dehydrogenase 2; JAK, Janus Kinase; Sec. Prog., Secretory Progenitor.

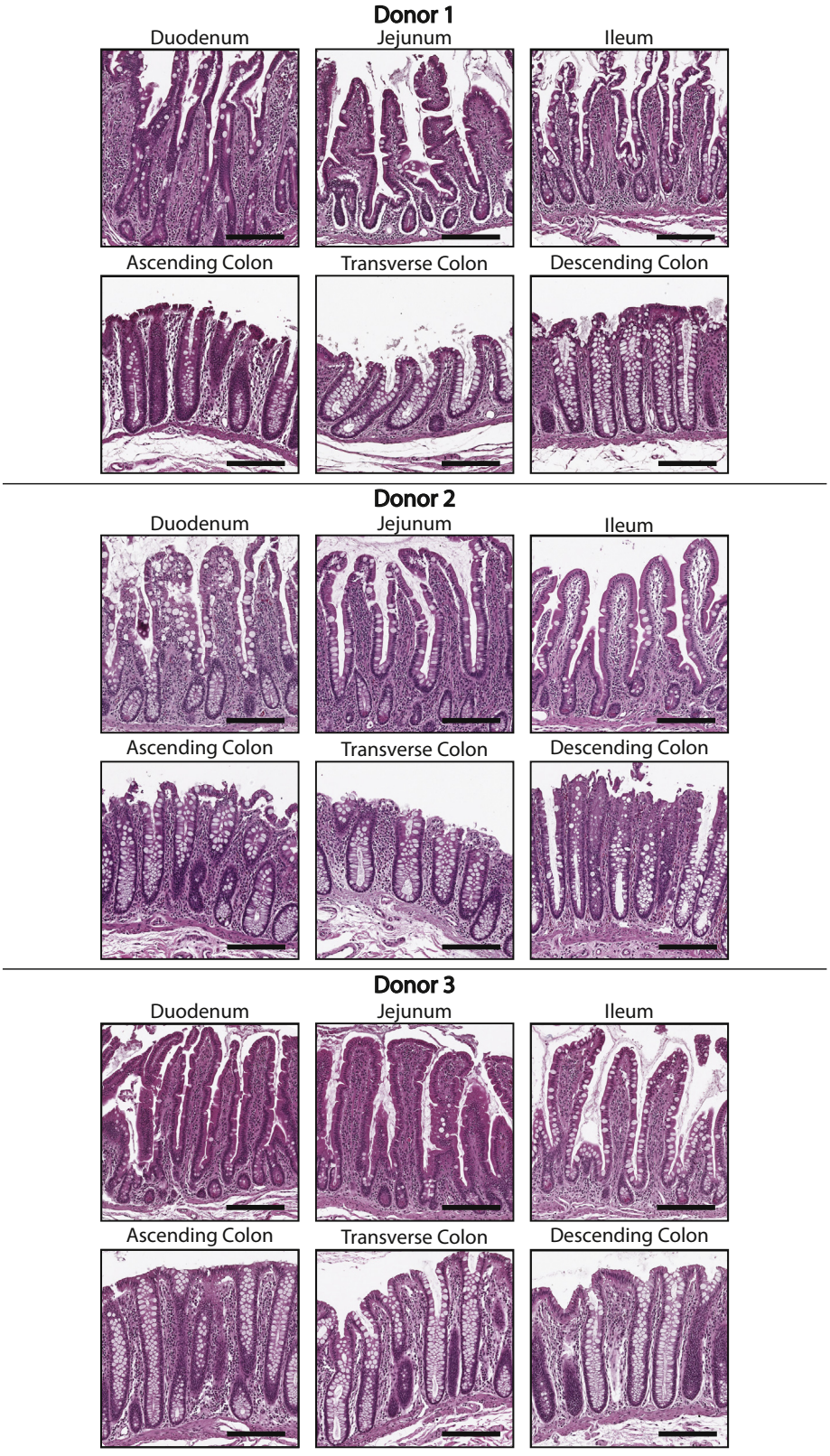

Figure 17. Tissue histology. H&E-stained tissues from each region for all 3 donors. *Scale bars*: 200 μm.

Our experimental design had many unique strengths. We used healthy transplant organ tissue from 3 adult male donors varying in age, race, and body mass index to characterize intestinal epithelial cells from duodenum through DC. DNA-oligo hashtag antibodies allowed a single library per donor for all 6 regions to be sequenced together,

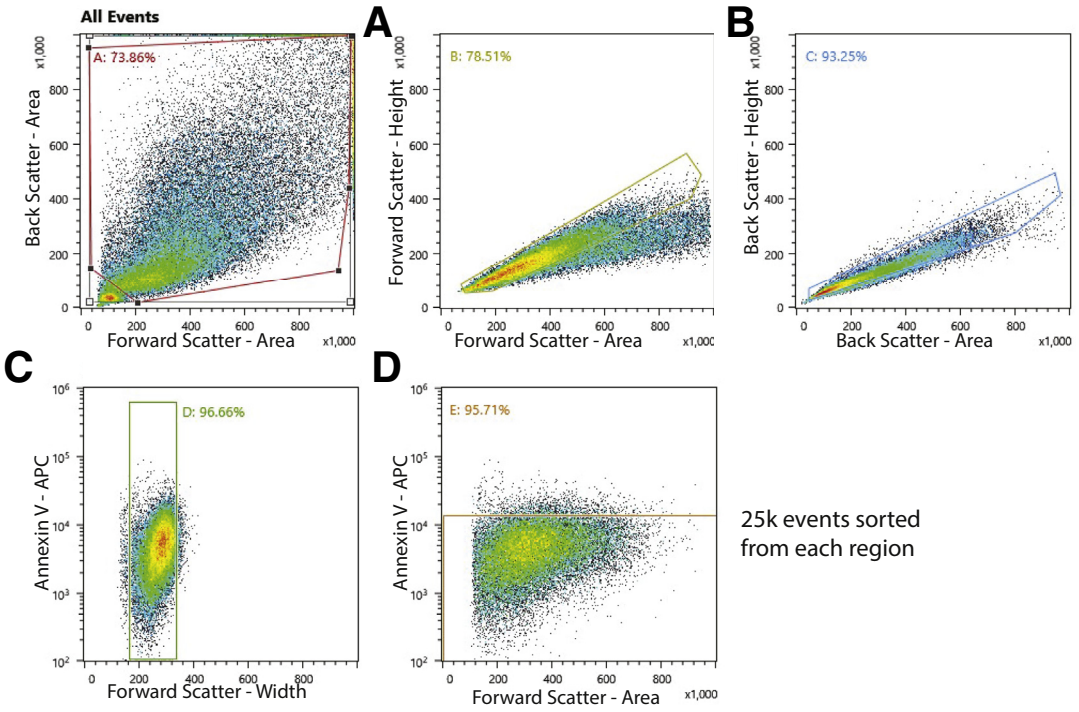

Figure 18. Fluorescence-activated cell sorter (FACS) strategy. FACS strategy for gating out cell fragments, likely doublets, and dead cells. APC, Allophycocyanin.

saving cost and avoiding intradonor batch effects while preserving biological variability. The hashtag antibodies also allowed for increased stringency when filtering for mutliplets and contamination. Analyzing cells across 6 regions allowed for comprehensive transcriptional signatures of genes significantly enriched in each lineage across the entire gut from 3 donors. We mapped cell cycle, mucins, hormones, transporters, digestive genes, and barrier function genes along the regions of the SI and colon. We showed drastic differences in PC growth factor expression from mouse literature and highlight the insufficiency of *LYZ* for uniquely marking human PCs. We used PAGA to infer a differentiation trajectory for each lineage and suggest organ-specific maturation for tuft and BEST4^{+} cells. We propose novel tuft cell interactions with pathogens and the immune system. Finally, our survey of receptors and primary drug targets across lineages highlights the utility and ease of our database to find previously undescribed gene expression. The regional differences found throughout our study highlight the importance of regional selection when studying the gut, yet many colonic scRNAseq studies do not specify the sample region or mention if pooled samples are from consistent regions. We hope our database serves as a resource to understand how drugs affect the intestinal epithelium and as guidance for future precision medicine approaches.

Methods

Donor Selection

Human donor intestines were received from 3 male organ donors, aged 29, 45, and 53 years (details in Figure 2), from HonorBridge (Formerly Carolina Donor Services, Durham, NC) with the following acceptance criteria: age $\leq$65 years, brain-dead only, human immunodeficiency virus negative, hepatitis negative, syphilis negative, tuberculosis negative, coronavirus disease-2019 negative, and no bowel surgery, severe abdominal injury, cancer, or chemotherapy. Pancreas donors were excluded to avoid duodenum loss. The University of North Carolina Institutional Review Board determined this study does not constitute human subjects research.

Tissue Processing

Intestines were transported on ice in University of Wisconsin Cold Storage Solution (Bridge to Life, Northbrook, IL). Tissue dissection began within 8 hours of cross-clamping. Fat/connective tissue were trimmed and intestinal regions were separated: duodenum (most-proximal 20 cm), jejunum/ileum splitting remaining SI, and colon split into thirds for AC/TC/DC (Figure 17). Two 3 $\times$ 3 cm mucosectomies were isolated from the center of each region for dissociation.

Mucosectomies were incubated in 10 mmol/L N-acetylcholine in Dulbecco's phosphate-buffered saline (dPBS) at room temperature for 30 minutes to remove mucus, then washed in ice-cold chelating buffer[141] + 100 μmol/L Y-27632. Tissues were incubated in chelating buffer with 2 mmol/L EDTA and 0.5 mmol/L dithiothreitol, then shaken to remove crypts. High-yield shakes were pooled by region, with SI shakes pooled to approximate 1:1 villus to crypt tissue by cell mass. Crypts and villi were dissociated to

Table 1. Reagents Used

	Company	Catalog number
Reagent		
N-acetylcholine	Millipore Sigma (St. Louis, MO)	A9165
dPBS	Gibco (Jenks, OK)	14190-144
Na2HPO4	Millipore-Sigma	S7907
KH2PO4	Millipore Sigma	P5655
NaCl	Millipore Sigma	S5886
KCl	Millipore Sigma	P5405
Sucrose	Fisher Scientific (Hampton, NH)	220-1
D-sorbitol	Fisher Scientific	439-500
Y27632	Selleck Chemical (Houston TX)	S6390
EDTA	Corning (Corning, NY)	46-034-CI
Dithiothreitol	Fisher Scientific	172-5
Protease VIII	Millipore Sigma	P5380
Advanced DMEM/F12	Gibco	12634-010
Bovine serum albumin	Fisher Scientific	BP1600-1
TotalSeq anti-human hashtag antibodies	BioLegend (San Diego, CA)	B0251-B0256
10% neutral buffered formalin	Fisher Scientific	22-050-105
Histo-clear	National Diagnostics (Atlanta, GA)	HS2001
Triton X-100	MP Biomedicals (Irvine, CA)	02194854-CF
Prolong Gold Antifade Reagent	Invitrogen (Waltham, MA)	P36930
Xylenes	Millipore-Sigma	534056
RNAscope Multiplex Fluorescent Reagent Kit v2	Advanced Cell Diagnotics (Newark, CA)	323100
Antibodies		
AnnexinV-APC	BioLegend	640920
Lysozyme	Diagnostic Biosystems (Pleasanton, CA)	RP028
CFTR	Cystic Fibrosis Foundation	A570
Mucin 2 (Ccp58)	Santa Cruz Biotechnology (Dallas, TX)	sc-7314
RAB27A	Proteintech (Rosemont, IL)	17817-1-AP
MUC5B	Millipore Sigma	HPA008246
FKBP1A	Thermo Fisher (Waltham, MA)	PA1-026A
IMPDH2	Proteintech	12948-1-AP
DHFR	Proteintech	15194-1-AP
Ki-67 monoclonal antibody (SolA15), APC	Invitrogen	17-5698-82
Donkey anti-rabbit IgG (H+L), Alexa Fluor 488	Invitrogen	A-21206
Cy3 AffiniPure F(ab')$_2$ fragment donkey anti-rabbit IgG (H+L)	Jackson Immunoresearch (West Grove, PA)	711-166-152
Alexa Fluor 647 AffiniPure donkey anti-mouse IgG (H+L)	Jackson Immunoresearch	715-605-150
Bisbenzamide	Millipore Sigma	14530
RNAscope probes		
Hs-SMOC2	Advanced Cell Diagnotics	533921
Hs-BEST4	Advanced Cell Diagnotics	481501
TSA cyanine 3 reagent pack	Akoya Biosciences (Marlborough, MA)	SAT704A001EA
TSA cyanine 5 reagent pack	Akoya Biosciences	SAT715A001EA

DMEM, Dulbecco's modified Eagle medium.

single cells using 4 mg/mL Protease VIII in dPBS + Y-27632 on ice for approximately 45 minutes with trituration via a P1000 micropipette every 10 minutes. Cells were checked under a light microscope and then filtered.

Sample Preparation

Single cells were washed with dPBS + Y-27632, resuspended in Advanced Dulbecco's modified Eagle medium/F12 + 1% bovine serum albumin + Y-27632, and then stained with AnnexinV-Allophycocyanin (APC) (1:100) and 1 TotalSeq Anti-Human Hashtag Antibody (1:100, Biolegend, San Diego, CA) per region to track all 6 regions with a single library preparation.[11] Cells were washed and resuspended in Advanced Dulbecco's modified Eagle medium + 1% bovine serum albumin + Y-27632 for sorting on a Sony Cell Sorter SH800Z (Sony, Tokyo, Japan) to enrich for live single epithelial cells (Figure 18). There were 25,000 cells that passed Annexin V live/dead parameters and were fluorescence-activated cell sorter isolated for each region, then different cell hashing antibodies were added to cells from each of the 6 regions before pooling for library preparation. An additional live/dead analysis was performed after pooling and approximately 10,000 cells from the pooled population were loaded onto the Chromium Next GEM Single Cell 3' GEM, Library and Gel Bead Kit v3.1 (PN-100012, 10x Genomics, Pleasanton, CA) for complementary DNA library preparation Sequencing was performed on an Illumina NextSeq 500 (Illumina, San Diego, CA).

Immunofluorescence and In Situ Hybridization

Tissue samples adjacent to the sections dissociated for single-cell dissociation were dissected from each region and

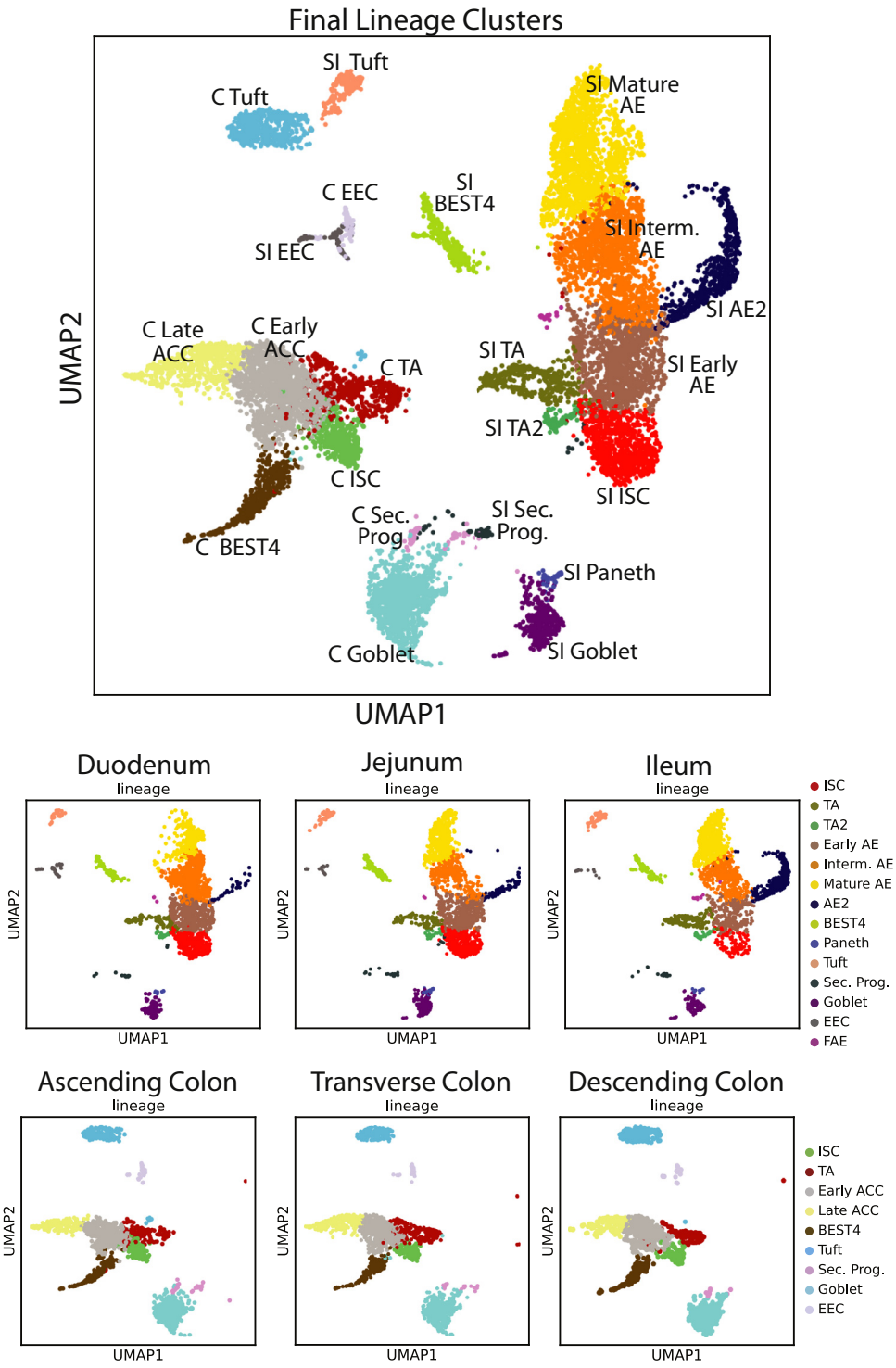

Figure 19. Final clusters shown by organ. *Top*: Final lineage clusters used for the rest of the analyses in our study. *Bottom*: Lineage clusters split by region. C, Colon; Interm., intermediate; Sec. Prog., Secretory Progentior; UMAP, Uniform Manifold Approximation and Projection.

then fixed in 10% neutral buffered formalin overnight at 4°C. The following day, tissues were washed 3 times in water and then stored in 70% ethanol until embedding in paraffin wax. Embedded tissues were sectioned onto glass slides.

For immunofluorescence, sections were deparaffinized and rehydrated using Histo-clear (Great Lakes IPM, Vestaburg, MI) and an ethanol gradient. Sections were permeabilized with 0.3% Triton X-100 (Thermo Fisher Scientific, Waltham, MA) for 20 minutes, then blocked with 3% bovine serum albumin for 30 minutes at room temperature. Sections then were incubated with primary antibodies (Table 1) in blocking buffer overnight at 4°C. The following day, the sections were washed in PBS and then

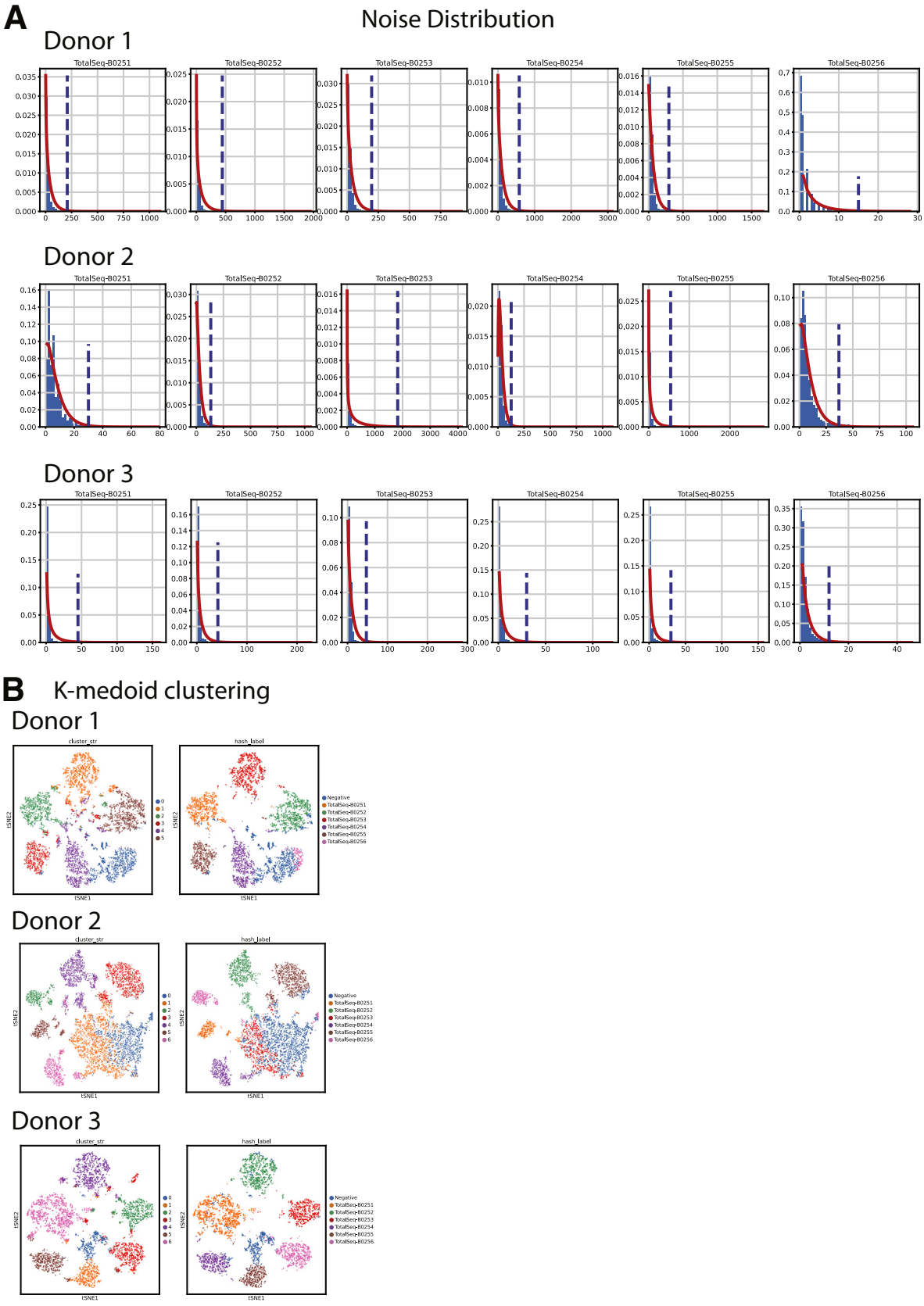

Figure 20. Hashtag deconvolution. (*A*) Per donor hashtag noise distributions. *Blue dotted lines* indicate the 99th percentile values for noise. Values above this line were called positive for a specific hashtag. (*B*) *Left*: K-medoid clustering for each donor based only on hashtag reads. Cells positive ($P < .01$) for multiple hashtags were removed as likely multiplets. Cells were called as negative if they did not surpass the noise threshold for all hashtags. *Right*: K-medoid clustering with final hashtag labeling for nonmultiplet cells.

Table 2. Table 2: Filtering Parameters

	Donor 1	Donor 2	Donor 3
Minimum genes	>500	>800	>500
Mitochondrial reads, %	<75	<50	<75
Minimum counts	>3000	>1000	>3000
Maximum counts	<50,000	<30,000	<50,000

incubated with secondary antibodies in blocking buffer for 1 hour at room temperature. Finally, slides were treated with bisbenzamide (MilliporeSigma, Burlington, MA) and coverslips were mounted using Prolong Gold Antifade Reagent (Thermo Fisher Scientific, Waltham, MA).

For in situ hybridization, sections were deparaffinized and rehydrated using xylenes and an ethanol gradient. In situ hybridization was performed using RNAscope (ACD Bio, Newark, CA) following the manufacturer's protocol (Table 1 lists the probes used). After the in situ hybridization, sections were co-stained for protein expression with immunofluorescence, following the protocol listed earlier, starting at the blocking step.

All sections were imaged on LSM 700 and LSM710 confocal microscopes (Zeiss, Jena, Germany), and figure preparation for images was completed using FIJI (National Institutes of Health, Bethesda, MD) and Adobe Illustrator (Adobe Inc., San Jose, CA).

Data Preparation and Hashtag Calling

Harmony (Harmonypy, v0.0.5) was used to integrate the top 40 principal components from each data set for clustering and visualization.[13] Leiden clustering was initialized with a k-nearest neighbor (kNN) graph (k = 10 neighbors) and a Leiden resolution of 0.92[14] to resolve most expected physiological lineages (Figure 19). Uniform Manifold Approximation and Projections (UMAPs) were initialized with PAGA embedding of Leiden clusters,[14,32] then nonepithelial EPCAM-negative lineages were eliminated. Regional hashtag deconvolution followed published methods: raw hashtag read counts were normalized using centered log ratio transformation followed by k-medoid clustering (k = 6 medoids for donor 1, k = 7 medoids for donors 2 and 3).[11] Hashtag noise distributions were determined by removing the highest-expressing cluster, then fitting a negative binomial distribution to the remaining cells. Cells were considered positive for a hashtag with counts above the distribution's 99th percentile ($P < .01$) threshold. Cells positive for multiple hashtags were excluded as likely doublets (Figure 20).

Data Processing, Filtering, Doublet Removal, and Feature Selection

After sequencing, single-cell fastq files were aligned to reference transcriptome GRCh38 with the 10× Cell Ranger pipeline (V4.0.0, 10x Genomics, Pleasanton, CA), and downstream analysis was performed with scanpy (v1.7.2)[142]. Annotations for cell-cycle phase predictions were added following previously published methods.[36] Quality filtering thresholds for each donor are shown in Table 2 and Figure 21. After filtering, read counts were log-transformed and normalized to the median read depth of donor 2, which had the fewest read counts. Variability resulting from gene expression count, mitochondrial percentage, and cell-cycle gene expression were regressed out by simple linear regression. Highly variable genes were identified with the Seurat method[143] (min_dispersion, 0.2; min_mean, 0.0125; max_mean, 6), identifying 2777 genes that subsequently were used for principal component analysis. Genes were scaled to have a mean of zero and unit variance.

Identifying Transcriptionally Distinct Subclusters

Subclustering was performed to isolate Paneth cells from SI goblet cells, which cluster together in the overall data set. For Paneth cells, the SI_*ITLN1*-high cluster was subset from the main data set and 40 principal components were recalculated and reharmonized. Leiden clusters were recalculated on the new principal components based on the same 2777 highly variable genes as the initial data set with Leiden resolution of 0.15 and k = 15 neighbors.

Further subclustering on SI and colon goblet cells was performed to show goblet cell heterogeneity in the SI and colon separately. For colon goblet cells, Leiden clustering settings were as follows: k = 5 nearest neighbors, Leiden resolution of 0.3, and 4000 highly variable genes were calculated based on 22 recomputed principal components from the colon goblet cells subset. For SI goblet cells, Leiden clustering settings were as follows: k = 10 nearest neighbors, Leiden resolution of 0.4, and 2000 highly variable genes were calculated based on 19 recomputed principal components on the SI goblet cell subset.

Online Databases

Human homologs for mouse genes were defined using Ensembl version release 104 (European [European Bioinformatics Institute, Cambridgeshire, UK] Bioinformatics Institute, Cambridgeshire, UK).[144] Pathway enrichment analysis was performed using Reactome,[91] with focus given to pathways with a false-discovery rate of less than 0.05, as calculated by over-representation analysis, and full reports are included as Supplementary Tables 3, 4, 6, and 7. Common drugs prescribed for ulcerative colitis and Crohn's disease were curated using online literature. Comprehensive receptor family lists and primary target genes for all approved drugs were downloaded from Guide to Pharmacology.[145] Phase I and phase II drug metabolism genes were defined via Reactome.[91]

Trajectory Analysis

To infer differentiation trajectories, subclustered cell populations were separated into SI and colon as previously described. For each data set, PAGA (v1.2) then was performed on a k-nearest neighbor graph of 20 neighbors

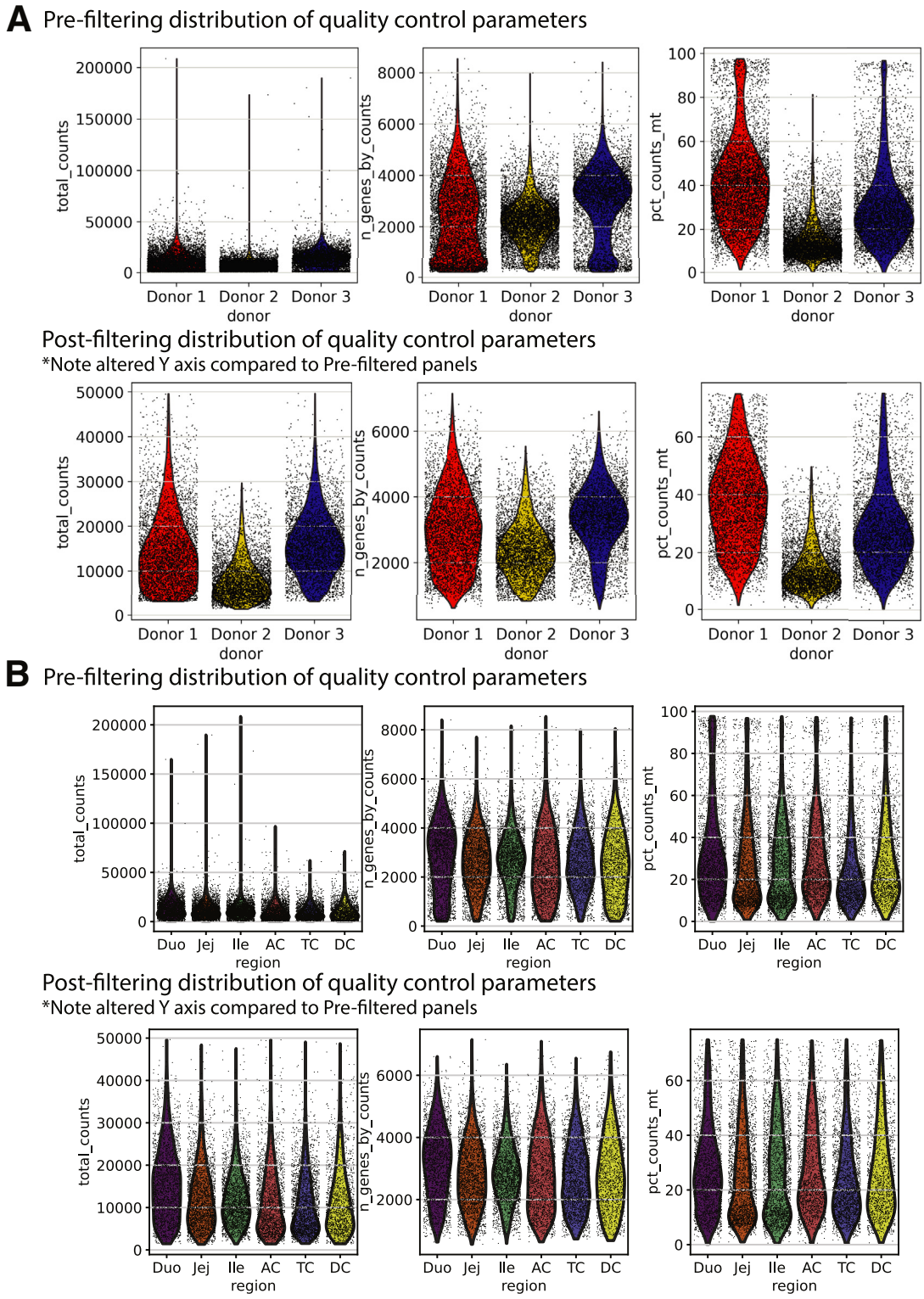

Figure 21. Filtering for cell quality. Total counts, N genes, and mitochondrial gene percentages shown for each donor before and after filtering; prefiltering (*top*) and postfiltering (*bottom*) by (*A*) donor and (*B*) region. Note differences in the Y axes between prefiltering and postfiltering *rows*. Duo, Duodenum; Ile, Ileum; Jej, Jejunum.

constructed from 40 principle components. The resultant transition connectivity matrix was filtered to remove spurious connections (SI, >0.08; colon, >0.09).

Differential Expression Analysis

To determine genes that consistently mark a lineage, as determined by previously described Leiden clustering, in all

3 donors, the data set first was separated into SI- and colon-specific data. For each organ, the depth-normalized expression of each gene was used to fit to a negative binomial general linear model with the diffxpy package (v0.7.4). A Wald test was used to iterate through all cell lineages, testing a null model in which only donor-specific batch effects were included: $x_i = \beta_0 + \beta_1 donor$ against an alternative model where a cell's inclusion in the current test lineage was included as a binary independent variable, correcting for multiple testing using the Benjamini–Hochberg procedure.

$$x_i = \beta_0 + \beta_1 donor + \beta_2 lineage$$

Each test then was repeated independently on each donor including at least 10 cells of the lineage, excluding donor as a covariate. A gene was determined to be a marker gene for a particular lineage if it met the following thresholds: (1) maximum expression in the lineage of interest, (2) q value less than 0.05 in the combined data set and all 3 donors individually, (3) minimum $\log_2$ fold-change (compared with the next highest expressing lineage) greater than 0.25, and (4) mean in-lineage normalized expression greater than 0.2.

References

1. Barker N. Adult intestinal stem cells: critical drivers of epithelial homeostasis and regeneration. Nat Rev Mol Cell Biol 2014;15:19–33.
2. Smillie CS, Biton M, Ordovas-Montanes J, Sullivan KM, Burgin G, Graham DB, Herbst RH, Rogel N, Slyper M, Waldman J, Sud M, Andrews E, Velonias G, Haber AL, Jagadeesh K, Vickovic S, Yao J, Stevens C, Dionne D, Nguyen LT, Villani AC, Hofree M, Creasey EA, Huang H, Rozenblatt-Rosen O, Garber JJ, Khalili H, Desch AN, Daly MJ, Ananthakrishnan AN, Shalek AK, Xavier RJ, Regev A. Intra- and inter-cellular rewiring of the human colon during ulcerative colitis. Cell 2019;178:714–730.e22.
3. Huang B, Chen Z, Geng L, Wang J, Liang H, Cao Y, Chen H, Huang W, Su M, Wang H, Xu Y, Liu Y, Lu B, Xian H, Li H, Li H, Ren L, Xie J, Ye L, Wang H, Zhao J, Chen P, Zhang L, Zhao S, Zhang T, Xu B, Che D, Si W, Gu X, Zeng L, Wang Y, Li D, Zhan Y, Delfouneso D, Lew AM, Cui J, Tang WH, Zhang Y, Gong S, Bai F, Yang M, Zhang Y. Mucosal profiling of pediatric-onset colitis and IBD reveals common pathogenics and therapeutic pathways. Cell 2019;179:1160–1176.e24.
4. Kanke M, Kennedy MM, Connelly S, et al. Single-cell analysis of colonic epithelium reveals unexpected shifts in cellular composition and molecular phenotype in treatment-naïve adult Crohn's disease. Cellular and Molecular Gastroenterology and Hepatology 2022. https://doi.org/10.1016/j.jcmgh.2022.02.005.
5. Parikh K, Antanaviciute A, Fawkner-Corbett D, Jagielowicz M, Aulicino A, Lagerholm C, Davis S, Kinchen J, Chen HH, Alham NK, Ashley N, Johnson E, Hublitz P, Bao L, Lukomska J, Andev RS, Bjorklund E, Kessler BM, Fischer R, Goldin R, Koohy H, Simmons A. Colonic epithelial cell diversity in health and inflammatory bowel disease. Nature 2019;567:49–55.
6. Wang Y, Song W, Wang J, Wang T, Xiong X, Qi Z, Fu W, Yang X, Chen YG. Single-cell transcriptome analysis reveals differential nutrient absorption functions in human intestine. J Exp Med 2020;217:e20191130.
7. Fujii M, Matano M, Toshimitsu K, Takano A, Mikami Y, Nishikori S, Sugimoto S, Sato T. Human intestinal organoids maintain self-renewal capacity and cellular diversity in niche-inspired culture condition. Cell Stem Cell 2018;23:787–793.e6.
8. Triana S, Stanifer ML, Metz-Zumaran C, Shahraz M, Mukenhirn M, Kee C, Serger C, Koschny R, Ordonez-Rueda D, Paulsen M, Benes V, Boulant S, Alexandrov T. Single-cell transcriptomics reveals immune response of intestinal cell types to viral infection. Mol Syst Biol 2021;17:e9833.
9. Busslinger GA, Weusten BLA, Bogte A, Begthel H, Brosens LAA, Clevers H. Human gastrointestinal epithelia of the esophagus, stomach, and duodenum resolved at single-cell resolution. Cell Rep 2021;34:108819.
10. Elmentaite R, Kumasaka N, Roberts K, Fleming A, Dann E, King HW, Kleshchevnikov V, Dabrowska M, Pritchard S, Bolt L, Vieira SF, Mamanova L, Huang N, Perrone F, Goh Kai'En I, Lisgo SN, Katan M, Leonard S, Oliver TRW, Hook CE, Nayak K, Campos LS, Dominguez Conde C, Stephenson E, Engelbert J, Botting RA, Polanski K, van Dongen S, Patel M, Morgan MD, Marioni JC, Bayraktar OA, Meyer KB, He X, Barker RA, Uhlig HH, Mahbubani KT, Saeb-Parsy K, Zilbauer M, Clatworthy MR, Haniffa M, James KR, Teichmann SA. Cells of the human intestinal tract mapped across space and time. Nature 2021;597:250–255.
11. Stoeckius M, Zheng S, Houck-Loomis B, Hao S, Yeung BZ, Mauck WM 3rd, Smibert P, Satija R. Cell Hashing with barcoded antibodies enables multiplexing and doublet detection for single cell genomics. Genome Biol 2018;19:224.
12. Elmentaite R, Ross ADB, Roberts K, James KR, Ortmann D, Gomes T, Nayak K, Tuck L, Pritchard S, Bayraktar OA, Heuschkel R, Vallier L, Teichmann SA, Zilbauer M. Single-cell sequencing of developing human gut reveals transcriptional links to childhood Crohn's disease. Dev Cell 2020;55:771–783 e5.
13. Korsunsky I, Millard N, Fan J, Slowikowski K, Zhang F, Wei K, Baglaenko Y, Brenner M, Loh PR, Raychaudhuri S. Fast, sensitive and accurate integration of single-cell data with Harmony. Nat Methods 2019;16:1289–1296.
14. Traag VA, Waltman L, van Eck NJ. From Louvain to Leiden: guaranteeing well-connected communities. Sci Rep 2019;9:5233.
15. Barker N, van Es JH, Kuipers J, Kujala P, van den Born M, Cozijnsen M, Haegebarth A, Korving J, Begthel H, Peters PJ, Clevers H. Identification of stem

cells in small intestine and colon by marker gene Lgr5. Nature 2007;449:1003–1007.
16. van der Flier LG, van Gijn ME, Hatzis P, Kujala P, Haegebarth A, Stange DE, Begthel H, van den Born M, Guryev V, Oving I, van Es JH, Barker N, Peters PJ, van de Wetering M, Clevers H. Transcription factor achaete scute-like 2 controls intestinal stem cell fate. Cell 2009; 136:903–912.
17. Whissell G, Montagni E, Martinelli P, Hernando-Momblona X, Sevillano M, Jung P, Cortina C, Calon A, Abuli A, Castells A, Castellvi-Bel S, Nacht AS, Sancho E, Stephan-Otto Attolini C, Vicent GP, Real FX, Batlle E. The transcription factor GATA6 enables self-renewal of colon adenoma stem cells by repressing BMP gene expression. Nat Cell Biol 2014;16:695–707.
18. Munoz J, Stange DE, Schepers AG, van de Wetering M, Koo BK, Itzkovitz S, Volckmann R, Kung KS, Koster J, Radulescu S, Myant K, Versteeg R, Sansom OJ, van Es JH, Barker N, van Oudenaarden A, Mohammed S, Heck AJ, Clevers H. The Lgr5 intestinal stem cell signature: robust expression of proposed quiescent '+4' cell markers. EMBO J 2012;31:3079–3091.
19. van der Flier LG, Haegebarth A, Stange DE, van de Wetering M, Clevers H. OLFM4 is a robust marker for stem cells in human intestine and marks a subset of colorectal cancer cells. Gastroenterology 2009; 137:15–17.
20. Gabut M, Bourdelais F, Durand S. Ribosome and translational control in stem cells. Cells 2020;9:497.
21. Woolnough JL, Atwood BL, Liu Z, Zhao R, Giles KE. The regulation of rRNA gene transcription during directed differentiation of human embryonic stem cells. PLoS One 2016;11:e0157276.
22. Zhang Q, Shalaby NA, Buszczak M. Changes in rRNA transcription influence proliferation and cell fate within a stem cell lineage. Science 2014;343:298–301.
23. Kristensen AR, Gsponer J, Foster LJ. Protein synthesis rate is the predominant regulator of protein expression during differentiation. Mol Syst Biol 2013;9:689.
24. Fu W, Liu Y, Yin H. Mitochondrial dynamics: biogenesis, fission, fusion, and mitophagy in the regulation of stem cell behaviors. Stem Cells Int 2019;2019:9757201.
25. Lu R, Markowetz F, Unwin RD, Leek JT, Airoldi EM, MacArthur BD, Lachmann A, Rozov R, Ma'ayan A, Boyer LA, Troyanskaya OG, Whetton AD, Lemischka IR. Systems-level dynamic analyses of fate change in murine embryonic stem cells. Nature 2009;462:358–362.
26. Avansino JR, Chen DC, Hoagland VD, Woolman JD, Stelzner M. Orthotopic transplantation of intestinal mucosal organoids in rodents. Surgery 2006; 140:423–434.
27. Fukuda M, Mizutani T, Mochizuki W, Matsumoto T, Nozaki K, Sakamaki Y, Ichinose S, Okada Y, Tanaka T, Watanabe M, Nakamura T. Small intestinal stem cell identity is maintained with functional Paneth cells in heterotopically grafted epithelium onto the colon. Genes Dev 2014;28:1752–1757.
28. Herring CA, Banerjee A, McKinley ET, Simmons AJ, Ping J, Roland JT, Franklin JL, Liu Q, Gerdes MJ, Coffey RJ, Lau KS. Unsupervised trajectory analysis of single-cell RNA-seq and imaging data reveals alternative tuft cell origins in the gut. Cell Syst 2018;6:37–51 e9.
29. van Es JH, Sato T, van de Wetering M, Lyubimova A, Yee Nee AN, Gregorieff A, Sasaki N, Zeinstra L, van den Born M, Korving J, Martens ACM, Barker N, van Oudenaarden A, Clevers H. Dll1+ secretory progenitor cells revert to stem cells upon crypt damage. Nat Cell Biol 2012;14:1099–1104.
30. Yang Q, Bermingham NA, Finegold MJ, Zoghbi HY. Requirement of Math1 for secretory cell lineage commitment in the mouse intestine. Science 2001; 294:2155–2158.
31. Sancho R, Cremona CA, Behrens A. Stem cell and progenitor fate in the mammalian intestine: Notch and lateral inhibition in homeostasis and disease. EMBO Rep 2015;16:571–581.
32. Wolf FA, Hamey FK, Plass M, Solana J, Dahlin JS, Gottgens B, Rajewsky N, Simon L, Theis FJ. PAGA: graph abstraction reconciles clustering with trajectory inference through a topology preserving map of single cells. Genome Biol 2019;20:59.
33. Gomez-Martinez I, Bliton RJ, Breau KA, Czerwinski M, Williamson IA, Wen J, Rawls JF, Magness ST. Transcriptomics informs design of a planar human enterocyte culture system that reveals metformin enhances fatty acid export. bioRXiv 2022.
34. Wille AC, Oliveira FA, Soares MA, Gomes JR. Cell cycle time and rate of entry of cells into mitosis in the small intestine of young rats. Cell Prolif 2004;37:189–194.
35. Gandara RM, Mahida YR, Potten CS. Regional differences in stem and transit cell proliferation and apoptosis in the terminal ileum and colon of mice after 12 Gy. Int J Radiat Oncol Biol Phys 2012;82:e521–e528.
36. Kowalczyk MS, Tirosh I, Heckl D, Rao TN, Dixit A, Haas BJ, Schneider RK, Wagers AJ, Ebert BL, Regev A. Single-cell RNA-seq reveals changes in cell cycle and differentiation programs upon aging of hematopoietic stem cells. Genome Res 2015;25:1860–1872.
37. Sato T, van Es JH, Snippert HJ, Stange DE, Vries RG, van den Born M, Barker N, Shroyer NF, van de Wetering M, Clevers H. Paneth cells constitute the niche for Lgr5 stem cells in intestinal crypts. Nature 2011; 469:415–418.
38. Holloway EM, Czerwinski M, Tsai YH, Wu JH, Wu A, Childs CJ, Walton KD, Sweet CW, Yu Q, Glass I, Treutlein B, Camp JG, Spence JR. Mapping development of the human intestinal niche at single-cell resolution. Cell Stem Cell 2020;28:568–580.e4.
39. Poulsen SS, Nexo E, Olsen PS, Hess J, Kirkegaard P. Immunohistochemical localization of epidermal growth factor in rat and man. Histochemistry 1986; 85:389–394.
40. Zhao J, de Vera J, Narushima S, Beck EX, Palencia S, Shinkawa P, Kim KA, Liu Y, Levy MD, Berg DJ, Abo A, Funk WD. R-spondin1, a novel intestinotrophic mitogen, ameliorates experimental colitis in mice. Gastroenterology 2007;132:1331–1343.
41. Shoshkes-Carmel M, Wang YJ, Wangensteen KJ, Toth B, Kondo A, Massasa EE, Itzkovitz S, Kaestner KH. Subepithelial telocytes are an important source of Wnts

that supports intestinal crypts. Nature 2018; 557:242–246.
42. Durand A, Donahue B, Peignon G, Letourneur F, Cagnard N, Slomianny C, Perret C, Shroyer NF, Romagnolo B. Functional intestinal stem cells after Paneth cell ablation induced by the loss of transcription factor Math1 (Atoh1). Proc Natl Acad Sci U S A 2012; 109:8965–8970.
43. Kim TH, Escudero S, Shivdasani RA. Intact function of Lgr5 receptor-expressing intestinal stem cells in the absence of Paneth cells. Proc Natl Acad Sci U S A 2012; 109:3932–3937.
44. Farin HF, Van Es JH, Clevers H. Redundant sources of Wnt regulate intestinal stem cells and promote formation of Paneth cells. Gastroenterology 2012;143:1518–1529 e7.
45. Haber AL, Biton M, Rogel N, Herbst RH, Shekhar K, Smillie C, Burgin G, Delorey TM, Howitt MR, Katz Y, Tirosh I, Beyaz S, Dionne D, Zhang M, Raychowdhury R, Garrett WS, Rozenblatt-Rosen O, Shi HN, Yilmaz O, Xavier RJ, Regev A. A single-cell survey of the small intestinal epithelium. Nature 2017;551:333–339.
46. Lu H, Ju DD, Yang GD, Zhu LY, Yang XM, Li J, Song WW, Wang JH, Zhang CC, Zhang ZG, Zhang R. Targeting cancer stem cell signature gene SMOC-2 overcomes chemoresistance and inhibits cell proliferation of endometrial carcinoma. EBioMedicine 2019; 40:276–289.
47. Jubb AM, Chalasani S, Frantz GD, Smits R, Grabsch HI, Kavi V, Maughan NJ, Hillan KJ, Quirke P, Koeppen H. Achaete-scute like 2 (ascl2) is a target of Wnt signalling and is upregulated in intestinal neoplasia. Oncogene 2006;25:3445–3457.
48. Schuijers J, Junker JP, Mokry M, Hatzis P, Koo BK, Sasselli V, van der Flier LG, Cuppen E, van Oudenaarden A, Clevers H. Ascl2 acts as an R-spondin/Wnt-responsive switch to control stemness in intestinal crypts. Cell Stem Cell 2015;16:158–170.
49. Salzman NH. Paneth cell defensins and the regulation of the microbiome: detente at mucosal surfaces. Gut Microbes 2010;1:401–406.
50. Haghverdi L, Buttner M, Wolf FA, Buettner F, Theis FJ. Diffusion pseudotime robustly reconstructs lineage branching. Nat Methods 2016;13:845–848.
51. Valentino MA, Lin JE, Snook AE, Li P, Kim GW, Marszalowicz G, Magee MS, Hyslop T, Schulz S, Waldman SA. A uroguanylin-GUCY2C endocrine axis regulates feeding in mice. J Clin Invest 2011; 121:3578–3588.
52. Cox HM. Neuropeptide Y receptors; antisecretory control of intestinal epithelial function. Auton Neurosci 2007; 133:76–85.
53. Wen J, Liu X, Qi Y, Niu F, Niu Z, Geng W, Zou Z, Huang R, Wang J, Zou H. BMP3 suppresses colon tumorigenesis via ActRIIB/SMAD2-dependent and TAK1/JNK signaling pathways. J Exp Clin Cancer Res 2019;38:428.
54. Holzer P, Reichmann F, Farzi A. Neuropeptide Y, peptide YY and pancreatic polypeptide in the gut-brain axis. Neuropeptides 2012;46:261–274.
55. Loh K, Herzog H, Shi YC. Regulation of energy homeostasis by the NPY system. Trends Endocrinol Metab 2015;26:125–135.
56. Kishi K, Takase S, Goda T. Enhancement of sucrase-isomaltase gene expression induced by luminally administered fructose in rat jejunum. J Nutr Biochem 1999;10:8–12.
57. Kalogeris TJ, Rodriguez MD, Tso P. Control of synthesis and secretion of intestinal apolipoprotein A-IV by lipid. J Nutr 1997;127:537S–543S.
58. Scheibner J, Trendelenburg AU, Hein L, Starke K, Blandizzi C. Alpha 2-adrenoceptors in the enteric nervous system: a study in alpha 2A-adrenoceptor-deficient mice. Br J Pharmacol 2002;135:697–704.
59. Si M, Lang J. The roles of metallothioneins in carcinogenesis. J Hematol Oncol 2018;11:107.
60. Klaassen CD, Liu J, Diwan BA. Metallothionein protection of cadmium toxicity. Toxicol Appl Pharmacol 2009; 238:215–220.
61. Coyle P, Philcox JC, Carey LC, Rofe AM. Metallothionein: the multipurpose protein. Cell Mol Life Sci 2002;59:627–647.
62. Ohgami RS, Campagna DR, McDonald A, Fleming MD. The Steap proteins are metalloreductases. Blood 2006; 108:1388–1394.
63. Anderson GJ, Frazer DM. Current understanding of iron homeostasis. Am J Clin Nutr 2017;106:1559S–1566S.
64. Schneider C, O'Leary CE, Locksley RM. Regulation of immune responses by tuft cells. Nat Rev Immunol 2019; 19:584–593.
65. O'Leary CE, Schneider C, Locksley RM. Tuft cells-systemically dispersed sensory epithelia integrating immune and neural circuitry. Ann Rev Immunol 2019; 37:47–72.
66. Nadjsombati MS, McGinty JW, Lyons-Cohen MR, Jaffe JB, DiPeso L, Schneider C, Miller CN, Pollack JL, Nagana Gowda GA, Fontana MF, Erle DJ, Anderson MS, Locksley RM, Raftery D, von Moltke J. Detection of succinate by intestinal tuft cells triggers a type 2 innate immune circuit. Immunity 2018;49:33–41 e7.
67. von Moltke J, Ji M, Liang HE, Locksley RM. Tuft-cell-derived IL-25 regulates an intestinal ILC2-epithelial response circuit. Nature 2016;529:221–225.
68. Howitt MR, Lavoie S, Michaud M, Blum AM, Tran SV, Weinstock JV, Gallini CA, Redding K, Margolskee RF, Osborne LC, Artis D, Garrett WS. Tuft cells, taste-chemosensory cells, orchestrate parasite type 2 immunity in the gut. Science 2016;351:1329–1333.
69. Gerbe F, van Es JH, Makrini L, Brulin B, Mellitzer G, Robine S, Romagnolo B, Shroyer NF, Bourgaux JF, Pignodel C, Clevers H, Jay P. Distinct ATOH1 and Neurog3 requirements define tuft cells as a new secretory cell type in the intestinal epithelium. J Cell Biol 2011; 192:767–780.
70. Bezençon C, Fürholz A, Raymond F, Mansourian R, Métairon S, Le Coutre J, Damak S. Murine intestinal cells expressing Trpm5 are mostly brush cells and express markers of neuronal and inflammatory cells. J Comp Neurol 2008;509:514–525.

71. Schneider C, O'Leary CE, von Moltke J, Liang HE, Ang QY, Turnbaugh PJ, Radhakrishnan S, Pellizzon M, Ma A, Locksley RM. A metabolite-triggered tuft cell-ILC2 circuit drives small intestinal remodeling. Cell 2018; 174:271–284 e14.
72. Roper SD, Chaudhari N. Taste buds: cells, signals and synapses. Nat Rev Neurosci 2017;18:485–497.
73. Kinnamon SC. Taste receptor signalling - from tongues to lungs. Acta Physiol (Oxf) 2012;204:158–168.
74. Vyas JM, Van der Veen AG, Ploegh HL. The known unknowns of antigen processing and presentation. Nat Rev Immunol 2008;8:607–618.
75. Kloetzel PM, Ossendorp F. Proteasome and peptidase function in MHC-class-I-mediated antigen presentation. Curr Opin Immunol 2004;16:76–81.
76. Barton GM, Kagan JC. A cell biological view of Toll-like receptor function: regulation through compartmentalization. Nat Rev Immunol 2009;9:535–542.
77. Lu Y-C, Yeh W-C, Ohashi PS. LPS/TLR4 signal transduction pathway. Cytokine 2008;42:145–151.
78. Hayashi F, Smith KD, Ozinsky A, Hawn TR, Yi EC, Goodlett DR, Eng JK, Akira S, Underhill DM, Aderem A. The innate immune response to bacterial flagellin is mediated by Toll-like receptor 5. Nature 2001; 410:1099–1103.
79. Bauer S, Kirschning CJ, Häcker H, Redecke V, Hausmann S, Akira S, Wagner H, Lipford GB. Human TLR9 confers responsiveness to bacterial DNA via species-specific CpG motif recognition. Proc Natl Acad Sci U S A 2001;98:9237–9242.
80. Xu M, Lu H, Lee YH, Wu Y, Liu K, Shi Y, An H, Zhang J, Wang X, Lai Y, Dong C. An interleukin-25-mediated autoregulatory circuit in keratinocytes plays a pivotal role in psoriatic skin inflammation. Immunity 2018; 48:787–798 e4.
81. Wald D, Qin J, Zhao Z, Qian Y, Naramura M, Tian L, Towne J, Sims JE, Stark GR, Li X. SIGIRR, a negative regulator of Toll-like receptor-interleukin 1 receptor signaling. Nat Immunol 2003;4:920–927.
82. Zhang C, Wu X, Zhao Y, Deng Z, Qian G. SIGIRR inhibits Toll-like receptor 4, 5, 9-mediated immune responses in human airway epithelial cells. Mol Biol Rep 2011; 38:601–609.
83. Qin J, Qian Y, Yao J, Grace C, Li X. SIGIRR inhibits interleukin-1 receptor- and Toll-like receptor 4-mediated signaling through different mechanisms. J Biol Chem 2005;280:25233–25241.
84. Schütz B, Ruppert A-L, Strobel O, Lazarus M, Urade Y, Büchler MW, Weihe E. Distribution pattern and molecular signature of cholinergic tuft cells in human gastrointestinal and pancreatic-biliary tract. Sci Rep 2019; 9:17466.
85. McGinty JW, Ting H-A, Billipp TE, Nadjsombati MS, Khan DM, Barrett NA, Liang H-E, Matsumoto I, von Moltke J. Tuft-cell-derived leukotrienes drive rapid anthelminth immunity in the small intestine but are dispensable for anti-protist immunity. Immunity 2020; 52:528–541.e7.
86. Grondin JA, Kwon YH, Far PM, Haq S, Khan WI. Mucins in intestinal mucosal defense and inflammation: learning from clinical and experimental studies. Front Immunol 2020;11:2054.
87. Sicard JF, Le Bihan G, Vogeleer P, Jacques M, Harel J. Interactions of intestinal bacteria with components of the intestinal mucus. Front Cell Infect Microbiol 2017;7:387.
88. Pelaseyed T, Bergstrom JH, Gustafsson JK, Ermund A, Birchenough GM, Schutte A, van der Post S, Svensson F, Rodriguez-Pineiro AM, Nystrom EE, Wising C, Johansson ME, Hansson GC. The mucus and mucins of the goblet cells and enterocytes provide the first defense line of the gastrointestinal tract and interact with the immune system. Immunol Rev 2014;260:8–20.
89. Pelaseyed T, Hansson GC. Membrane mucins of the intestine at a glance. J Cell Sci 2020;133:jcs240929.
90. Ma J, Rubin BK, Voynow JA. Mucins, mucus, and goblet cells. Chest 2018;154:169–176.
91. Jassal B, Matthews L, Viteri G, Gong C, Lorente P, Fabregat A, Sidiropoulos K, Cook J, Gillespie M, Haw R, Loney F, May B, Milacic M, Rothfels K, Sevilla C, Shamovsky V, Shorser S, Varusai T, Weiser J, Wu G, Stein L, Hermjakob H, D'Eustachio P. The reactome pathway knowledgebase. Nucleic Acids Res 2020; 48:D498–D503.
92. Cornick S, Tawiah A, Chadee K. Roles and regulation of the mucus barrier in the gut. Tissue Barriers 2015;3: e982426.
93. Layunta E, Javerfelt S, Dolan B, Arike L, Pelaseyed T. IL-22 promotes the formation of a MUC17 glycocalyx barrier in the postnatal small intestine during weaning. Cell Rep 2021;34:108757.
94. Sun WW, Krystofiak ES, Leo-Macias A, Cui R, Sesso A, Weigert R, Ebrahim S, Kachar B. Nanoarchitecture and dynamics of the mouse enteric glycocalyx examined by freeze-etching electron tomography and intravital microscopy. Commun Biol 2020;3:5.
95. Nyström EEL, Martinez-Abad B, Arike L, Birchenough GMH, Nonnecke EB, Castillo PA, Svensson F, Bevins CL, Hansson GC, Johansson MEV. An intercrypt subpopulation of goblet cells is essential for colonic mucus barrier function. Science 2021;372: eabb1590.
96. Birchenough GM, Johansson ME, Gustafsson JK, Bergstrom JH, Hansson GC. New developments in goblet cell mucus secretion and function. Mucosal Immunol 2015;8:712–719.
97. Beumer J, Puschhof J, Bauza-Martinez J, Martinez-Silgado A, Elmentaite R, James KR, Ross A, Hendriks D, Artegiani B, Busslinger GA, Ponsioen B, Andersson-Rolf A, Saftien A, Boot C, Kretzschmar K, Geurts MH, Bar-Ephraim YE, Pleguezuelos-Manzano C, Post Y, Begthel H, van der Linden F, Lopez-Iglesias C, van de Wetering WJ, van der Linden R, Peters PJ, Heck AJR, Goedhart J, Snippert H, Zilbauer M, Teichmann SA, Wu W, Clevers H. High-resolution mRNA and secretome atlas of human enteroendocrine cells. Cell 2020; 181:1291–1306 e19.

98. Billing LJ, Larraufie P, Lewis J, Leiter A, Li J, Lam B, Yeo GS, Goldspink DA, Kay RG, Gribble FM, Reimann F. Single cell transcriptomic profiling of large intestinal enteroendocrine cells in mice - identification of selective stimuli for insulin-like peptide-5 and glucagon-like peptide-1 co-expressing cells. Mol Metab 2019;29:158–169.
99. Roberts GP, Larraufie P, Richards P, Kay RG, Galvin SG, Miedzybrodzka EL, Leiter A, Li HJ, Glass LL, Ma MKL, Lam B, Yeo GSH, Scharfmann R, Chiarugi D, Hardwick RH, Reimann F, Gribble FM. Comparison of human and murine enteroendocrine cells by transcriptomic and peptidomic profiling. Diabetes 2019; 68:1062–1072.
100. Sjolund K, Sanden G, Hakanson R, Sundler F. Endocrine cells in human intestine: an immunocytochemical study. Gastroenterology 1983;85:1120–1130.
101. Liddle RA. Neuropods. Cell Mol Gastroenterol Hepatol 2019;7:739–747.
102. Kaelberer MM, Buchanan KL, Klein ME, Barth BB, Montoya MM, Shen X, Bohorquez DV. A gut-brain neural circuit for nutrient sensory transduction. Science 2018; 361:eaat5236.
103. Bellono NW, Bayrer JR, Leitch DB, Castro J, Zhang C, O'Donnell TA, Brierley SM, Ingraham HA, Julius D. Enterochromaffin cells are gut chemosensors that couple to sensory neural pathways. Cell 2017; 170:185–198 e16.
104. Worthington JJ, Reimann F, Gribble FM. Enteroendocrine cells-sensory sentinels of the intestinal environment and orchestrators of mucosal immunity. Mucosal Immunol 2018;11:3–20.
105. Gribble FM, Reimann F. Signalling in the gut endocrine axis. Physiol Behav 2017;176:183–188.
106. Egerod KL, Engelstoft MS, Grunddal KV, Nohr MK, Secher A, Sakata I, Pedersen J, Windelov JA, Fuchtbauer EM, Olsen J, Sundler F, Christensen JP, Wierup N, Olsen JV, Holst JJ, Zigman JM, Poulsen SS, Schwartz TW. A major lineage of enteroendocrine cells coexpress CCK, secretin, GIP, GLP-1, PYY, and neurotensin but not somatostatin. Endocrinology 2012; 153:5782–5795.
107. Habib AM, Richards P, Cairns LS, Rogers GJ, Bannon CA, Parker HE, Morley TC, Yeo GS, Reimann F, Gribble FM. Overlap of endocrine hormone expression in the mouse intestine revealed by transcriptional profiling and flow cytometry. Endocrinology 2012; 153:3054–3065.
108. Kiela PR, Ghishan FK. Physiology of intestinal absorption and secretion. Best Pract Res Clin Gastroenterol 2016;30:145–159.
109. Dawson PA, Karpen SJ. Intestinal transport and metabolism of bile acids. J Lipid Res 2015; 56:1085–1099.
110. Imamura T, Kitamoto Y. Expression of enteropeptidase in differentiated enterocytes, goblet cells, and the tumor cells in human duodenum. Am J Physiol Gastrointest Liver Physiol 2003;285:G1235–G1241.
111. Lu Z, Ding L, Lu Q, Chen Y-H. Claudins in intestines: distribution and functional significance in health and diseases. Tissue Barriers 2013;1:e24978.
112. Camilleri M. Leaky gut: mechanisms, measurement and clinical implications in humans. Gut 2019;68:1516–1526.
113. Koutroubakis IE. Recent advances in the management of distal ulcerative colitis. World J Gastrointest Pharmacol Ther 2010;1:43–50.
114. Ahmad R, Rah B, Bastola D, Dhawan P, Singh AB. Obesity-induces organ and tissue specific tight junction restructuring and barrier deregulation by claudin switching. Sci Rep 2017;7:5125.
115. Zhu C, Chen Z, Jiang Z. Expression, distribution and role of aquaporin water channels in human and animal stomach and intestines. Int J Mol Sci 2016;17:1399.
116. Jorgensen PB, Fenton TM, Morbe UM, Riis LB, Jakobsen HL, Nielsen OH, Agace WW. Identification, isolation and analysis of human gut-associated lymphoid tissues. Nat Protoc 2021;16:2051–2067.
117. Dillon A, Lo DD. M cells: intelligent engineering of mucosal immune surveillance. Front Immunol 2019; 10:1499.
118. Hase K, Ohshima S, Kawano K, Hashimoto N, Matsumoto K, Saito H, Ohno H. Distinct gene expression profiles characterize cellular phenotypes of follicle-associated epithelium and M cells. DNA Res 2005; 12:127–137.
119. Terahara K, Yoshida M, Igarashi O, Nochi T, Pontes GS, Hase K, Ohno H, Kurokawa S, Mejima M, Takayama N, Yuki Y, Lowe AW, Kiyono H. Comprehensive gene expression profiling of Peyer's patch M cells, villous M-like cells, and intestinal epithelial cells. J Immunol 2008; 180:7840–7846.
120. Nakato G, Fukuda S, Hase K, Goitsuka R, Cooper MD, Ohno H. New approach for m-cell-specific molecules screening by comprehensive transcriptome analysis. DNA Res 2009;16:227–235.
121. Lo D, Tynan W, Dickerson J, Scharf M, Cooper J, Byrne D, Brayden D, Higgins L, Evans C, O'Mahony DJ. Cell culture modeling of specialized tissue: identification of genes expressed specifically by follicle-associated epithelium of Peyer's patch by expression profiling of Caco-2/Raji co-cultures. Int Immunol 2004;16:91–99.
122. Kimura S, Kobayashi N, Nakamura Y, Kanaya T, Takahashi D, Fujiki R, Mutoh M, Obata Y, Iwanaga T, Nakagawa T, Kato N, Sato S, Kaisho T, Ohno H, Hase K. Sox8 is essential for M cell maturation to accelerate IgA response at the early stage after weaning in mice. J Exp Med 2019;216:831–846.
123. Nakamura Y, Kimura S, Hase K. M cell-dependent antigen uptake on follicle-associated epithelium for mucosal immune surveillance. Inflamm Regen 2018;38:15.
124. Mercado-Lubo R, McCormick BA. A unique subset of Peyer's patches express lysozyme. Gastroenterology 2010;138:36–39.
125. Zhao X, Sato A, Dela Cruz CS, Linehan M, Luegering A, Kucharzik T, Shirakawa AK, Marquez G, Farber JM, Williams I, Iwasaki A. CCL9 is secreted by the follicle-associated epithelium and recruits dome region Peyer's patch CD11b+ dendritic cells. J Immunol 2003; 171:2797–2803.
126. Hua S. Advances in oral drug delivery for regional targeting in the gastrointestinal tract - influence of

physiological, pathophysiological and pharmaceutical factors. Front Pharmacol 2020;11:524.
127. Thelen K, Dressman JB. Cytochrome P450-mediated metabolism in the human gut wall. J Pharm Pharmacol 2009;61:541–558.
128. Speer JE, Wang Y, Fallon JK, Smith PC, Allbritton NL. Evaluation of human primary intestinal monolayers for drug metabolizing capabilities. J Biol Eng 2019;13:82.
129. Iswandana R, Irianti MI, Oosterhuis D, Hofker HS, Merema MT, de Jager MH, Mutsaers HAM, Olinga P. Regional differences in human intestinal drug metabolism. Drug Metab Dispos 2018;46:1879–1885.
130. Philpott HL, Nandurkar S, Lubel J, Gibson PR. Drug-induced gastrointestinal disorders. Frontline Gastroenterol 2014;5:49–57.
131. Wang D, Zou L, Jin Q, Hou J, Ge G, Yang L. Human carboxylesterases: a comprehensive review. Acta Pharm Sin B 2018;8:699–712.
132. Ando Y, Saka H, Asai G, Sugiura S, Shimokata K, Kamataki T. UGT1A1 genotypes and glucuronidation of SN-38, the active metabolite of irinotecan. Ann Oncol 1998;9:845–847.
133. Pitot HC, Adjei AA, Reid JM, Sloan JA, Atherton PJ, Rubin J, Alberts SR, Duncan BA, Denis L, Schaaf LJ, Yin D, Sharma A, McGovren P, Miller LL, Erlichman C. A phase I and pharmacokinetic study of a powder-filled capsule formulation of oral irinotecan (CPT-11) given daily for 5 days every 3 weeks in patients with advanced solid tumors. Cancer Chemother Pharmacol 2006; 58:165–172.
134. Rothenberg ML, Kuhn JG, Schaaf LJ, Drengler RL, Eckhardt SG, Villalona-Calero MA, Hammond L, Miller LL, Petit RG, Rowinsky EK, Von Hoff DD. Alternative dosing schedules for irinotecan. Oncology (Williston Park) 1998;12:68–71.
135. Kumler I, Sorensen PG, Palshof J, Hogdall E, Skovrider-Ruminski W, Theile S, Fullerton A, Nielsen PG, Jensen BV, Nielsen DL. Oral administration of irinotecan in patients with solid tumors: an open-label, phase I, dose escalating study evaluating safety, tolerability and pharmacokinetics. Cancer Chemother Pharmacol 2019; 83:169–178.
136. Harnik Y, Buchauer L, Ben-Moshe S, Averbukh I, Levin Y, Savidor A, Eilam R, Moor AE, Itzkovitz S. Spatial discordances between mRNAs and proteins in the intestinal epithelium. Nat Metab 2021;3:1680–1693.
137. Panes J, Vermeire S, Lindsay JO, Sands BE, Su C, Friedman G, Zhang H, Yarlas A, Bayliss M, Maher S, Cappelleri JC, Bushmakin AG, Rubin DT. Tofacitinib in patients with ulcerative colitis: health-related quality of life in phase 3 randomised controlled induction and maintenance studies. J Crohns Colitis 2018; 12:145–156.
138. Sanders DB, Hart IK, Mantegazza R, Shukla SS, Siddiqi ZA, De Baets MH, Melms A, Nicolle MW, Solomons N, Richman DP. An international, phase III, randomized trial of mycophenolate mofetil in myasthenia gravis. Neurology 2008;71:400–406.
139. Kremer JM, Cohen S, Wilkinson BE, Connell CA, French JL, Gomez-Reino J, Gruben D, Kanik KS, Krishnaswami S, Pascual-Ramos V, Wallenstein G, Zwillich SH. A phase IIb dose-ranging study of the oral JAK inhibitor tofacitinib (CP-690,550) versus placebo in combination with background methotrexate in patients with active rheumatoid arthritis and an inadequate response to methotrexate alone. Arthritis Rheum 2012; 64:970–981.
140. Seyhan AA, Carini C. Are innovation and new technologies in precision medicine paving a new era in patients centric care? J Transl Med 2019;17:114.
141. Wang Y, Gunasekara DB, Reed MI, DiSalvo M, Bultman SJ, Sims CE, Magness ST, Allbritton NL. A microengineered collagen scaffold for generating a polarized crypt-villus architecture of human small intestinal epithelium. Biomaterials 2017;128:44–55.
142. Wolf F Alexander, Angerer Philipp, Theis Fabian J. SCANPY: large-scale single-cell gene expression data analysis. Genome Biology 2018;19:15.
143. Satija R, Farrell JA, Gennert D, Schier AF, Regev A. Spatial reconstruction of single-cell gene expression data. Nat Biotechnol 2015;33:495–502.
144. Howe KL, Achuthan P, Allen J, Allen J, Alvarez-Jarreta J, Amode MR, Armean IM, Azov AG, Bennett R, Bhai J, Billis K, Boddu S, Charkhchi M, Cummins C, Da Rin Fioretto L, Davidson C, Dodiya K, El Houdaigui B, Fatima R, Gall A, Garcia Giron C, Grego T, Guijarro-Clarke C, Haggerty L, Hemrom A, Hourlier T, Izuogu OG, Juettemann T, Kaikala V, Kay M, Lavidas I, Le T, Lemos D, Gonzalez Martinez J, Marugan JC, Maurel T, McMahon AC, Mohanan S, Moore B, Muffato M, Oheh DN, Paraschas D, Parker A, Parton A, Prosovetskaia I, Sakthivel MP, Salam AIA, Schmitt BM, Schuilenburg H, Sheppard D, Steed E, Szpak M, Szuba M, Taylor K, Thormann A, Threadgold G, Walts B, Winterbottom A, Chakiachvili M, Chaubal A, De Silva N, Flint B, Frankish A, Hunt SE, GR II, Langridge N, Loveland JE, Martin FJ, Mudge JM, Morales J, Perry E, Ruffier M, Tate J, Thybert D, Trevanion SJ, Cunningham F, Yates AD, Zerbino DR, Flicek P. Ensembl 2021. Nucleic Acids Res 2021;49:D884–D891.
145. Armstrong JF, Faccenda E, Harding SD, Pawson AJ, Southan C, Sharman JL, Campo B, Cavanagh DR, Alexander SPH, Davenport AP, Spedding M, Davies JA, Nc I. The IUPHAR/BPS guide to pharmacology in 2020: extending immunopharmacology content and introducing the IUPHAR/MMV guide to malaria pharmacology. Nucleic Acids Res 2020;48: D1006–D1021.

Received November 29, 2021. Accepted February 7, 2022.

Correspondence
Address correspondence to: Scott T. Magness, PhD, Department of Biomedical Engineering, University of North Carolina at Chapel Hill, 111 Mason Farm Road, Chapel Hill, North Carolina e-mail: magness@med.unc.edu.

Acknowledgments
The authors first thank the organ donors without whom our study would have been impossible. The authors thank HonorBridge (formerly Carolina Donor Services) for assistance in coordinating organ donations. The authors thank Gabrielle Cannon at the Advanced Analytics core at the University of North Carolina Chapel Hill and Ashley Ezzell at the Histology Research Core at the University of North Carolina Chapel Hill. The authors thank Michael

Czerwinski for help with dissociation and computation, Nathan Kohn and Willow Liu for assistance with dissociation, and Laurianne Van Landeghem for reviewing the manuscript. We further thank the UNC Cystic Fibrosis Center for the CFTR antibody. This publication is part of the Human Cell Atlas - www.humancellatlas.org/publications

CRediT Authorship Contributions

Joseph Burclaff, Ph.D. (Data curation: Lead; Formal analysis: Lead; Visualization: Lead; Writing – original draft: Lead; Writing – review & editing: Lead)

R. Jarrett Bliton, B.S. (Data curation: Lead; Formal analysis: Lead; Software: Lead; Visualization: Lead; Writing – original draft: Lead; Writing – review & editing: Lead)

Keith A Breau, B.S. (Data curation: Lead; Formal analysis: Lead; Software: Lead;Visualization: Lead; Writing – original draft: Supporting)

Meryem T Ok, B.S. (Data curation: Supporting; Formal analysis: Supporting; Visualization: Supporting; Writing – original draft: Supporting)

Ismael Gomez-Martinez, B.S. (Formal analysis: Supporting; Visualization: Supporting)

Jolene S Ranek, B.S. (Software: Supporting; Writing – review & editing: Supporting)

Aadra P Bhatt, Ph.D. (Writing – review & editing: Supporting; Intellectual contributions: Supporting)

Jeremy E Purvis, Ph.D. (Writing – review & editing: Supporting)

John T Woosley, MD (Data analysis: Supporting)

Scott T Magness, Ph.D. (Conceptualization: Lead; Funding acquisition: Lead; Supervision: Lead; Writing – review & editing: Equal)

Data Availability Statement

Data will be available in the NCBI Gene Expression Omnibus, accession number: GSE185224. Python Scripts allowing for main steps of our analysis to be performed will be available on GitHub.

Conflicts of interest

The authors disclose no conflicts.

Funding

Supported by National Institutes of Health grants R01DK115806, R01DK109559, P30-DK034987, P30-DK065988, and the Katherine E. Bullard Charitable Trust for Gastrointestinal Stem Cell and Regenerative Research (S.T.M.), F32DK124929 (J.B.), T32-GM133364 (K.A.B), and F31-HL156433 and 5T32-GM067553 (J.S.R.). Also supported by a Career Development Award from the Crohn's and Colitis Foundation, and the University Cancer Research Fund (A.P.B.).